THE ASTROPHYSICAL JOURNAL, 526:505–522, 1999 November 20

ON HEATING THE SUN'S CORONA BY MAGNETIC EXPLOSIONS: FEASIBILITY IN ACTIVE REGIONS AND PROSPECTS FOR QUIET REGIONS AND CORONAL HOLES

R. L. MOORE,[1] D. A. FALCONER,[2] J. G. PORTER,[1] AND S. T. SUESS[1]

Received 1998 December 24; accepted 1999 July 2

ABSTRACT

We build a case for the persistent strong coronal heating in active regions and the pervasive quasi-steady heating of the corona in quiet regions and coronal holes being driven in basically the same way as the intense transient heating in solar flares: by explosions of sheared magnetic fields in the cores of initially closed bipoles.

We begin by summarizing the observational case for exploding sheared core fields being the drivers of a wide variety of flare events, with and without coronal mass ejections. We conclude that the arrangement of an event's flare heating, whether there is a coronal mass ejection, and the time and place of the ejection relative to the flare heating are all largely determined by four elements of the form and action of the magnetic field: (1) the arrangement of the impacted, interacting bipoles participating in the event, (2) which of these bipoles are active (have sheared core fields that explode) and which are passive (are heated by injection from impacted active bipoles), (3) which core field explodes first, and (4) which core-field explosions are confined within the closed field of their bipoles and which ejectively open their bipoles.

We then apply this magnetic-configuration framework for flare heating to the strong coronal heating observed by the *Yohkoh* Soft X-ray Telescope in an active region with strongly sheared core fields observed by the Marshall Space Flight Center vector magnetograph. All of the strong coronal heating is in continually microflaring sheared core fields or in extended loops rooted against these active core fields. Thus, the strong heating occurs in field configurations consistent with the heating being driven by frequent core-field explosions that are smaller than but similar to those in confined flares and flaring arches. From analysis of the thermal and magnetic energetics of two selected core-field microflares and a bright extended loop, we find that (1) it is energetically feasible for the sheared core fields to drive all of the coronal heating in the active region via a staccato of magnetic microexplosions, (2) the microflares at the feet of the extended loop behave as the flares at the feet of flaring arches in that more coronal heating is driven within the active bipole than in the extended loop, (3) the filling factor of the X-ray plasma in the core field microflares and in the extended loop is ~ 0.1, and (4) to release enough magnetic energy for a typical microflare (10^{27}–10^{28} ergs), a microflaring strand of sheared core field need expand and/or untwist by only a few percent at most.

Finally, we point out that (1) the field configurations for strong coronal heating in our example active region (i.e., neutral-line core fields, many embedded in the feet of extended loops) are present in abundance in the magnetic network in quiet regions and coronal holes, and (2) it is known that many network bipoles do microflare and that many produce detectable coronal heating. We therefore propose that exploding sheared core fields are the drivers of most of the heating and dynamics of the solar atmosphere, ranging from the largest and most powerful coronal mass ejections and flares, to the vigorous microflaring and coronal heating in active regions, to the multitude of fine-scale explosive events in the magnetic network, which drive microflares, spicules, global coronal heating, and, consequently, the solar wind.

Subject headings: MHD — Sun: corona — Sun: magnetic fields — Sun: X-rays, gamma rays

1. INTRODUCTION

It has long been known from eclipse observations that the Sun's outer atmosphere, the corona, is far-reaching and impressively structured. The streamers seen in the outer corona suggest outflow. Observations in space show that the outer corona does in fact continually flow outward, expanding and accelerating to become the supersonic and super-Alfvènic solar wind that fills the heliosphere, reaching far beyond the planets. The inner corona, the corona at heights less than about half a solar radius, is roughly hydrostatic and has a density scale height of about 1/10 of a solar radius, several hundred times the scale height in the photosphere, indicating that the corona is hundreds of times hotter than the photosphere (Allen 1973; Moore et al. 1991). That the corona has such a high temperature is made obvious by X-ray images of the Sun, such as those from *Yohkoh*; that the corona glows in soft X-rays requires temperatures in excess of 10^6 K (Acton 1996). To first order, the Sun has an extended corona and solar wind and continually emits X-rays because it somehow keeps its outer atmosphere heated to million-degree temperatures (Parker 1963; Withbroe 1992). While this has been recognized for decades, the heating process remains obscure and persists as a fundamental puzzle of solar astrophysics.

In this paper we consider the nonuniform (non–spherically symmetric) structure of the solar atmosphere for

[1] Marshall Space Flight Center, Space Science Laboratory, SD5O, Huntsville, AL 35812.
[2] University of Alabama, Huntsville, Department of Physics, Huntsville, AL 35899.

clues to the heating process. All of the nonuniform structure of the solar atmosphere above the photosphere is imposed by magnetic field that is rooted in and below the photosphere and permeates the atmosphere above; the structure of the upper atmosphere reflects the structure of the magnetic field. The broad stance of this paper is that the magnetic structure is a key to the heating process. We find that, somewhat as the streamers of the outer corona are true flags of the outflow that feeds the solar wind, so too does the magnetic structure in and below the inner corona have basic implications for the heating process there.

The heating that sustains the hot corona and solar wind occurs continually and globally, both in the magnetically closed regions and in the magnetically open regions (coronal holes). Superposed on this ubiquitous quasi-steady activity are flares and coronal mass ejections, sporadic local outbursts of much stronger coronal heating, and/or coronal mass expulsion. In the most powerful of these events, the total energy released is of order 10^{32} ergs, the total mass ejected is of order 10^{16} g, and the rates of heating and mass expulsion transiently exceed those of the entire nonflaring corona (Sturrock 1980; Withbroe & Noyes 1977; Holzer 1992). All sizeable flares and coronal mass ejections (event energy $>10^{30}$ ergs) are born within the closed coronal magnetic fields in the streamer belt, that is, in active regions or in the magnetically weaker but larger helmet arcades under streamers, never in the open fields of coronal holes (Svestka 1976; Gosling 1996).

Flares and coronal mass ejections obviously have broadly similar origins: in addition to being seated only in closed magnetic regions, both are evidently powered by explosive releases of magnetic energy from the fields in which they occur (Sturrock 1980; Moore 1988; Low 1996). Beyond these broad similarities, the physical relationship of flares and coronal mass ejections remains rather unsettled and controversial (Kahler 1992; Gosling 1993; Hudson, Haisch, & Strong 1995; Gosling 1995). The issue is controversial partly because of nomenclature and partly because of the complexity and variety of events in which flares occur jointly with coronal mass ejections. The signature that qualifies an event to be called a flare is a burst of coronal and chromospheric radiation resulting from a burst of heating (often involving bursts of particle acceleration); the signature that qualifies an event to be called a coronal mass ejection is the eruptive motion and/or disappearance of material (e.g., a streamer blowout, or an ejective filament eruption or flare spray) marking the ejection of mass from the inner corona out into the solar wind (e.g., Moore et al. 1980; Rust et al. 1980; Hudson et al. 1996; Low 1996). Of these events, an energetically large one in an active region always produces a strong flare (strong heating) and often simultaneously launches a large fast coronal mass ejection from the flare site (Moore 1988; Moore, La Rosa, & Orwig 1995). These tandem events are commonly called eruptive flares or, more precisely, ejective flares (Svestka, Jackson, & Machado 1992; Machado et al. 1988a; Moore & Roumeliotis 1992); such tandem events might equally well be called flaring coronal mass ejections. The physically pertinent question is whether the flare heating is the cause of the mass ejection or the mass ejection is the cause of the flare heating, or, rather than either being the cause of the other, both have the same basic cause, the cause of the overall coordinated event. The situation is further complicated by the observations that many events produce a flare but no coronal mass ejection, other events produce a large coronal mass ejection with no noticeable flare, and in many tandem events, while a flare does occur nearly simultaneously with the coronal mass ejection, the lateral span of the mass ejection is many times that of the flare and the mass ejection is not centered on the site of the flare (Kahler 1987, 1992; Gopalswamy 1999). So, except that a closed magnetic field is the setting and energy source of the events, about all that is widely agreed upon concerning the relation between flares and coronal mass ejections is that (1) not all events produce both a flare and a coronal mass ejection and (2) the relation between the flare and the mass ejection is not the same in all events in which both occur.

The significance of flares and coronal mass ejections for the present paper is that they are releases of magnetic energy that (except for some coronal mass ejections) produce strong coronal heating. This suggests that the magnetic structure of flares and coronal mass ejections might provide clues to coronal heating in general. Our approach is to follow Machado et al. (1988a) in considering the magnetic field configurations that give rise to flares and coronal mass ejections and the strong coronal heating in them. This yields a field-configuration framework that plausibly accounts for the observed range of relationships between flares and coronal mass ejections and that gives configurational rules for the location and driving of the flare heating within the magnetic field. In this framework, the magnetic configuration of any given flare and/or coronal mass ejection event consists of a single closed bipole or two or more impacted closed bipoles, and the mass motion and heating in the event is driven by explosive eruption of sheared magnetic field in the core of at least one of the bipoles. We then consider the quasi-steady strong coronal heating observed in active regions, note that it fits naturally into the magnetic framework for flares and coronal mass ejections, and, from this, construct a plausible magnetic picture for the coronal heating in active regions. In this picture, most coronal heating in active regions is driven by core-field microexplosions, that is, by localized flarelike eruptive activity in low-lying sheared magnetic fields rooted along polarity inversion lines in the magnetic flux. We show that this picture is energetically feasible for the sheared core fields and strong coronal heating observed in an example active region. Finally, the picture for coronal heating in active regions is extended to the heating of the global corona everywhere outside of active regions, the heating here being driven by magnetic microexplosions in neutral-line core fields in the magnetic network. The energetic feasibility of the proposed picture for heating the corona in quiet regions and coronal holes will be addressed in a subsequent paper in a manner similar to that for active regions in the present paper.

2. A TEMPLATE FOR CORONAL HEATING: MAGNETIC FIELD CONFIGURATIONS FOR FLARES AND CORONAL MASS EJECTIONS

Since flares and coronal mass ejections are releases of magnetic energy, it is plausible that the basic components and dynamics of any one of these events are set by the magnetic field configuration in which the event arises. Specifically, it seems natural that there should be different field configurations that allow or prevent the occurrence of tandem events, and that, of those configurations that allow

tandem events, there should be different configurations that give different relations between the flare and the coronal mass ejection. This idea is fostered in part by the observation that every large long-duration flare (having a soft X-ray burst that lasts for 6 hr or more above the background flux from the full-disk nonflaring corona) is accompanied by a coronal mass ejection (Shelley et al. 1983). The flares in these events are also known as two-ribbon eruptive flares (Svestka et al. 1992). These events all have basically the same pre-event magnetic field configuration: a large (lateral extent $>10^5$ km) closed bipole in which the core field (the field rooted near the polarity inversion line and forming the core or inner tunnel of the overall magnetic arcade) is strongly sheared and hence contains a large store of nonpotential magnetic energy (Moore 1987, 1988; Moore & Roumeliotis 1992; Moore et al. 1995). The sheared core field is often rendered partially visible in chromospheric images by chromospheric-temperature plasma held within the sheared core field at and above chromospheric heights. This cool plasma is seen as a long filament lying above and running along the polarity dividing line of the bipoles's photospheric magnetic flux. Before the event, the filament shows the direction and form of the central part of the sheared core field on which the filament material is strung. During the event, because the filament material is carried with the field that threads it, the filament material is a visible tracer of the motion and changing form of this part of the sheared core field as it erupts (Moore 1987, 1988; Kahler et al. 1988; Moore & Roumeliotis 1992). The event begins with the onset of the ejective eruption of the whole bipole, including much of the sheared core field (Moore & LaBonte 1980; Moore et al. 1997). The flare heating is centered under the erupting core field and reaches its peak only after the core-field (filament) eruption and enveloping coronal mass ejection are well underway (Kahler et al. 1988; Hiei, Hundhausen, & Sime 1993); the heating apparently results from reconnection in the wake of the eruption (Moore et al. 1980; Moore & LaBonte 1980; Moore & Roumeliotis 1992; Low 1996). So, in these events it is clear that the flare heating is not the cause of the coronal mass ejection. Instead, both the expulsion of the coronal and filament plasma and the early flare heating are magnetically driven by the ejective eruption and opening of the sheared-core magnetic bipole, and the long-lasting flare heating comes from the reconnection in the reclosing of the opened field (Moore & LaBonte 1980; Kahler et al. 1988; Moore 1988; Low 1996; Moore et al. 1997). More to the point, these events all have basically the same pre-event field configuration (a sheared-core bipole), and the flare and coronal mass ejection have a set temporal and spatial relation, their joint development being coordinated by the eruptive self-opening of the sheared-core bipole. Thus, these events encourage the idea that the configuration of the magnetic field determines the basic character of the energy-release events within it. More specifically, these single-bipole tandem events suggest that for tandem events in which there is a different timing or placement of the flare relative to the mass ejection, the pre-event configuration is something other than a single large sheared-core bipole. (As we discuss in Appendix A, these different tandem events have magnetic configurations composed of two impacted bipoles, each with its own sheared core field. One bipole explodes first and triggers in the impacted bipole another shared-core-field explosion. The two-bipole magnetic configurations of these tandem events are expressions of the active-active case depicted symbolically in Figure 6.)

Machado & Moore (1986) and Machado et al. (1988a) found further evidence that the broad heating and eruptive-motion aspects of an energy-release event are set by the configuration of the magnetic field. They examined the magnetic field configuration of 23 flare events by combining sequences of X-ray images of each event with vector magnetograms of the active region in which the event happened. Additional information came from sequences of chromospheric images of some of these events and of some other events. From these observations, Machado et al. (1988a) proposed a framework for classifying flare/coronal mass ejection events in terms of the magnetic field configuration. Because all of the events studied by Machado et al. (1988a) occurred in magnetic configurations composed of two or more impacted bipoles, they did not explicitly include single-bipole events in their classification system. However, as we describe in Appendix A, single-bipole events fit naturally into the system. With the inclusion of single-bipole events, this classification system encompasses all flare events, with or without coronal mass ejections, and explicitly indicates the relation between the flare and coronal mass ejection in events that have both.

The conclusions that are drawn from observations of single-bipole events (e.g., Moore 1988; Moore & Roumeliotis 1992) and from observations of multiple-bipole events (Machado et al. 1988a) and that are the basis of our expanded version of the Machado et al. (1988a) magnetic-configuration event classification system can be summarized as follows:

1. Most flare events are multiple-bipole events rather than single-bipole events. A single-bipole event is one in which the flare heating is limited to a single magnetic bipole; that is, all of the flare loops cross a single neutral line between two contiguous regions of opposite magnetic polarity. In a multiple-bipole event, two or more impacted bipoles (each with its own neutral line) are involved. The flare heating in these bipoles develops in close coordination through interaction between the impacted bipoles.

2. Each bipole in an event is either active or passive. An active bipole is one that is heated more by release of its own internal magnetic energy than by injection of energetic particles and hot plasma from interaction with impacted bipoles. A passive bipole is one that is heated less by internal magnetic energy release than by interaction with impacted active bipoles. Every multiple-bipole event has at least one active bipole, and in every single-bipole event the bipole is necessary an active bipole.

3. Active bipoles have a markedly nonpotential internal magnetic field, seen in vector magnetograms and in chromospheric and coronal images as shear and twist deformation relative to the potential field computed from the observed line-of-sight component of the photospheric roots of the field. Usually the shear is concentrated in the core of the bipole, the degree of shear being greatest along the neutral line and decreasing away so that the field in the outer envelope of the bipole is much less sheared than the core field. Passive bipoles display little or no magnetic shear or twist.

4. Most of the flare heating in an event is in the active bipoles; each active bipole heats itself more than it heats its impacted passive bipoles. Of the active bipoles in an event, those having the greater stored magnetic energy (indicated

by the product of the strength, shear, and extent of the core field) have the greater heating.

5. The magnetic energy release in an active bipole is either confined or ejective. In a confined release, there is writhing motion and rapid restructuring of the twisted core field within the bipole. This action may trigger energy release in impacted active bipoles or drive reconnection and energy injection at interfaces with impacted bipoles, but the active bipole remains closed throughout the event. In an ejective release, much of the twisted core, along with the outer envelope of the bipole, is eruptively expelled from the initially closed body of the bipole. This action can also drive interactions with impacted bipoles similar to those driven by confined releases. An ejective release in a large sheared-core bipole produces a coronal mass ejection from that bipole along with a long-duration two-ribbon flare in that bipole.

6. The magnetic energy release in an event begins either within an active bipole or at an interface of an active bipole with an impacted bipole. Any other impacted bipoles in the event join in through interaction with the initiating active bipole or its impacted bipoles.

For the coronal heating in flares, our field-configuration framework amounts to the following three rules: (1) The strongest flare heating in an event occurs within an active bipole. (2) A flaring active bipole can drive weaker but substantial flare heating, together with surging mass motion, in a passive bipole impacted against it. (3) Most flare heating is driven by eruptive action (either confined or ejective) of the sheared core fields in active bipoles. In the next section, we show that much of the nonflare quasi-steady strong coronal heating in active regions plausibly follows these same rules. We point out observations of magnetic structure, fine-scale magnetic activity, and coronal heating that together support the view that most of the heating that sustains the quasi-steady corona in active regions is similar to the strong transient coronal heating in flares in that it too is driven by eruptive events in the cores of active bipoles. For the quasi-steady heating, the eruptive events are much smaller and much more numerous than flare-sized eruptions. These magnetic microexplosions drive heating within themselves as in single-bipole flares. If the microflaring core field is in a bipole that is embedded in the roots of much larger magnetic loops, then it can drive coronal heating in them as in our active-passive case for flare heating in impacted bipoles (see Appendix A).

3. CORONAL HEATING BY MAGNETIC MICROEXPLOSIONS IN ACTIVE REGIONS

As we discussed above, according to the observations of Machado et al. (1988a), sheared core magnetic fields are apparently the source of most flares in active regions, the flare heating being a consequence of explosive release of nonpotential magnetic energy from the core field. That sheared core fields are evidently the energy source of the cataclysmic heating in flares naturally suggests that they may also be the energy source of much of the strong quasi-steady coronal heating in active regions. That is, since it is observed that sheared core fields often explode to produce flares, it is reasonable to expect that when these fields are not exploding in full-fledged flares they might gradually "leak" their stored energy to fuel the sustained coronal heating in active regions. This possibility has been investigated by the solar group at the Marshall Space Flight Center (MSFC) by registering *Yohkoh* SXT coronal X-ray images with MSFC vector magnetograms of active regions (Moore et al. 1994; Falconer et al. 1997; Porter, Falconer, & Moore 1998). These superposed images show that most of the more strongly heated (brighter) coronal X-ray features rooted in active regions either trace out or stem from around strongly sheared core fields, as in the example active region in Figure 1. Hence, it appears that sheared core fields are indeed major sources of coronal heating in active regions.

3.1. *Example Active Region*

The X-ray image in Figure 1 is not a single exposure, but a so-called persistent-brightness image distilled from a series of exposures distributed over a *Yohkoh* orbit, all taken with the same filter and normalized to the same exposure time. The brightness of each pixel in the persistent-brightness image is the minimum for that pixel through the normalized series. The particular set of normalized images used to construct the persistent-brightness image of Figure 1 are the 10 complete frames of the 12 frame sequence in Figure 2. Falconer et al. (1997) found that most of the brighter features in persistent-brightness images of active regions can be sorted into two classes: core features and extended loops. Core features are confined to low-lying core magnetic fields closely enveloping neutral lines in the magnetic flux, whereas extended loops arch higher and can have one end rooted far from any neutral line. By these criteria, features A, B, E, and F in Figure 1 are all core features; A and B reside in the core field hugging the neutral line of the overall bipole of the active region, while E and F are in the core field encasing the neutral line around an island of positive polarity in the negative-polarity domain of the overall bipole. Features C and D are good examples of persistently strongly heated extended loops. The intervals of strong neutral-line magnetic shear mapped in Figure 1 and the alignment of core features A and B with the neutral line show that the bright core features in this active region were embedded in strongly sheared core fields. It is also seen that one end of the two extended loops was rooted around the strongly sheared core field of the magnetic island. Thus, this example active region points insistently to sheared core fields as sources of strong coronal heating.

By construction, the persistent-brightness image shows all those coronal X-ray features that remained bright throughout the entire sun-viewing portion of the orbit, an interval of about 50 minutes. Also by construction, the persistent-brightness image gives no indication of whether a feature varied significantly in brightness or structure during the orbit, but the presence or absence of such short-term changes can be directly assessed from the original sequence of snapshots from which the persistent-brightness image is extracted. Figure 2 shows that the core features in our example active region underwent many noticeable changes in brightness and substructure in the few-minute intervals between frames. In contrast, the extended coronal loops were much steadier, changing hardly at all from frame to frame. Apparently, there was continual microflaring in the sheared core fields but little such activity in the extended loops. This again suggests that the sheared core fields are the source of the strong coronal heating both within the core fields and in the bright loops extending from around the magnetic island. Further, the observed core-field micro-

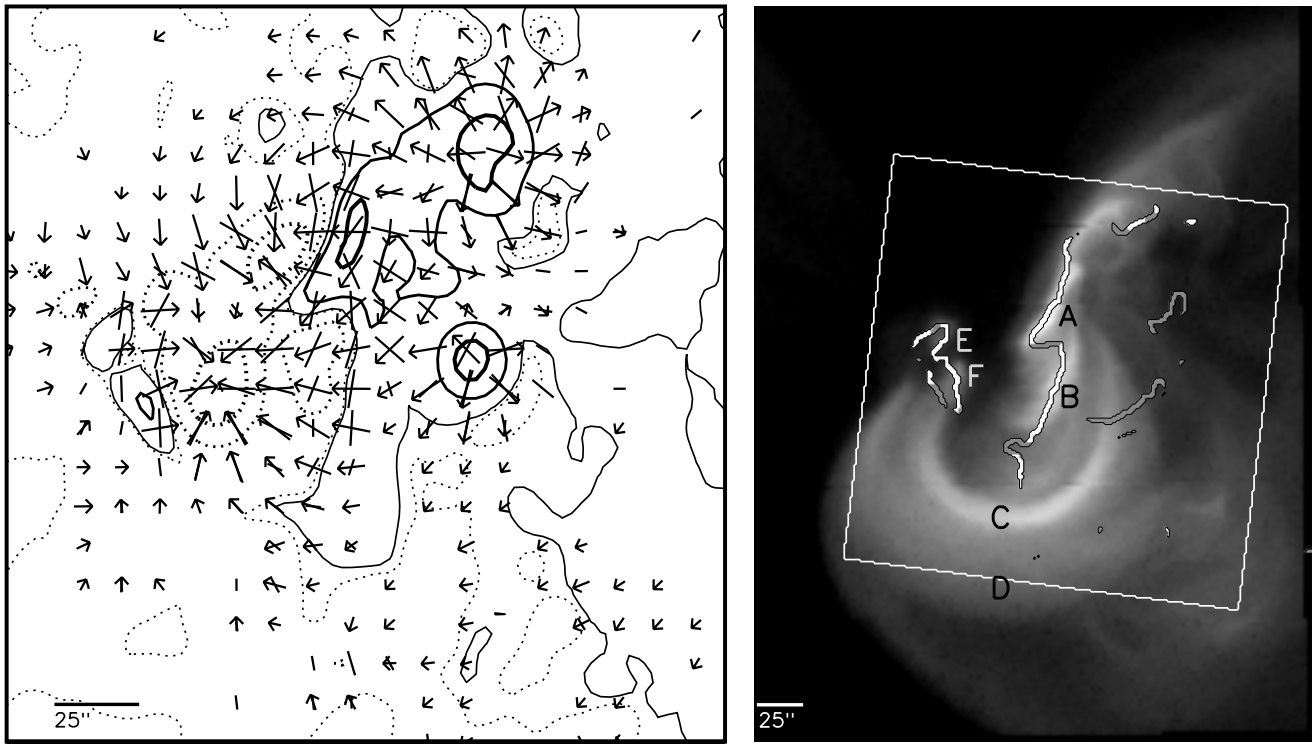

FIG. 1.—Example active region showing strong coronal heating rooted in and around strongly sheared core fields. *Left*: MSFC vector magnetogram with computed potential transverse field (*arrows*) superposed. The greater the shear angle (defined as the acute angle between the observed transverse field [*dashes*] and the potential transverse field), the greater the nonpotentiality of the observed field. The weakest transverse fields shown are 150 G; the strongest are ≥ 500 G. The strength of the line-of-sight field component is mapped by the contours (*solid contours*, positive polarity; *dotted contours*, negative polarity; 25, 500, and 1500 G levels). *Right*: Persistent-brightness coronal X-ray image (extracted from the sequence of images in Fig. 2) superposed on the neutral-line shear map derived from the vector magnetogram in the left panel. The tilted square is the field of view of the left panel. The neutral-line magnetic shear map displays only those neutral-line segments on which both the observed and the potential transverse fields are above 150 G. The magnetic shear is stronger in the white segments of the neutral lines (shear angle $>45°$) than in the gray segments (shear angle $<45°$). (Modified from Falconer et al. 1997).

flaring in Figure 2 suggests to us that it is core-field activity of this type by which the energy stored in the sheared core field is continually released to sustain the heating (Moore et al. 1994; Porter et al. 1994; Falconer et al. 1997; Porter et al. 1998).

3.2. *Model*

To delve into the feasibility of our hypothesis that the long-term strong coronal heating in active regions is driven by microflaring activity in sheared core fields, we need at least a conceptual model for the magnetic energy release in a core-field microflare event. For this, we assume that the microflare events are basically similar to the many full-fledged flares in which the energy release is apparently driven by explosive eruption and expansion of much of the sheared core field spanning the flare (Moore 1988). That is, we assume that each of the microflare brightenings in Figure 2 marks a magnetic microexplosion, an explosion of the strand of sheared core field that brightens. The microflare events in the sheared core field along the main neutral line of our example active region seem to be confined; they do not appear to eject magnetic field out of the core. So, we take these events to be confined microexplosions, miniature versions of confined eruptive flares. On the other hand, some microexplosions in the sheared core field around the magnetic island might be ejective in the manner of ejective flaring arch events (described in the Appendix A). That is, in these microexplosions some of the exploding core field might eject itself up into the leg of an adjacent extended loop, the foot of the leg being impacted against the embedded active bipole encircling the magnetic island.

For either a confined microexplosion or an ejective one, the picture that we have in mind for the initiation of the explosion of the strand of sheared core field is essentially the same. This picture is sketched in Figure 3 for a confined explosion, patterned after the confined filament-eruption flare presented by Moore (1988). We start with a stable strand of sheared core field as in the top sketch in Figure 3. We suppose that the convectively driven flows in and below the photosphere (i.e., the flows in and of the photospheric granules) randomly push together adjacent opposite-polarity feet of sheared field lines at the neutral line, forcing them to reconnect as the two flux clumps merge and cancel. This "tether cutting" both weakens the tying of the sheared field to the photosphere and increases the twist (winding and braiding) in the field above the photosphere, as indicated in the second sketch in Figure 3. This "floating twist" builds up until the strand becomes unstable, eruptively kinking or herniating, and driving reconnection that reduces the winding/braiding of the field. This results in strong heating of the plasma in the reconnecting field, and releases some of the reconnected field to expand upward (third sketch in Fig. 3). In a confined explosion, none of the exploding field is ejected and the end product is a less twisted, stable strand of sheared core field holding hot plasma, as in the bottom sketch in Figure 3. In an ejective explosion, some of the erupting strand herniates far out of the core field in which the explosion is seated; it then recon-

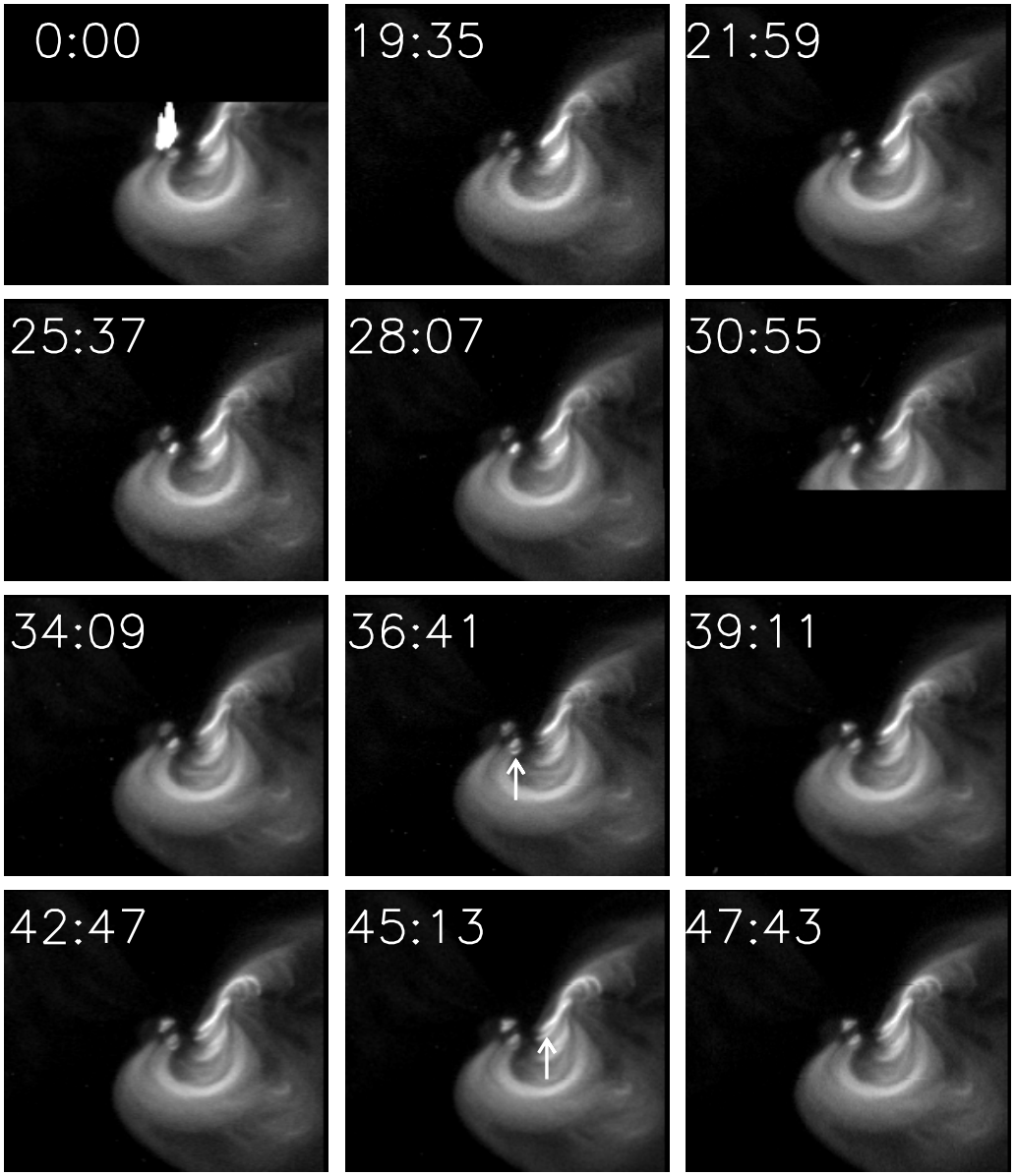

FIG. 2.—Sequence of coronal X-ray images of our example active region showing that, in contrast to the much steadier brightness and substructure of the extended bright loops, the sheared core fields continually microflare. For the orbit that covered the time of the magnetogram in Fig. 1, these are all of the images of this active region taken by the *Yohkoh* SXT in partial frame mode with the thin aluminium filter and exposures of 338 or 168 ms. All frames have been normalized to the same brightness scale to remove apparent brightness changes caused by changes in exposure time. Each framed is labeled with its time lapse (minutes: seconds) from the first frame. The arrows in the eighth and eleventh frames point out the two microflares for which we analyze the energetics.

nects with itself (reclosing) and with impacted surrounding fields. The final result within the core field is the same as in the bottom sketch in Figure 3. For either a confined explosion or an ejective explosion, some heating is also driven in impacted surrounding fields (not shown in Fig. 3).

While some of the magnetic energy released in a microexplosion dissipates into heat via the reconnection, much of the rest goes into work on the surroundings via the expansion of the released field. We expect that both the reconnection and the expansion generated MHD waves that propagate and dissipate beyond the exploding strand of core field. This expectation is consistent with the observed enhancements in the corona in and around our example active region. Because the X-ray images in Figures 1 and 2 have square-root scaling of the brightness, they show only the brighter coronal X-ray features in the interior of our active region. Logarithmic scaling of the brightness shows a halo of less strong—but still obviously enhanced—coronal heating all around the embedded brighter features seen in Figures 1 and 2 (e.g., see Fig. 1 of Falconer et al. 1997). In addition, the logarithmic images show several noticeably enhanced large coronal loops stemming from around the magnetic island in our active region and arching to remote regions far to the east. If microexplosions in the sheared core fields are the source of the heating in these various enhanced extensive coronal features in and around our active region, then it is clear that a substantial part of the energy released in these explosions is transported far outside the core fields and that some of the energy is deposited on magnetic field lines not threading the explosions.

Our scenario for the driving of coronal heating by core-field microexplosions in our example active region is

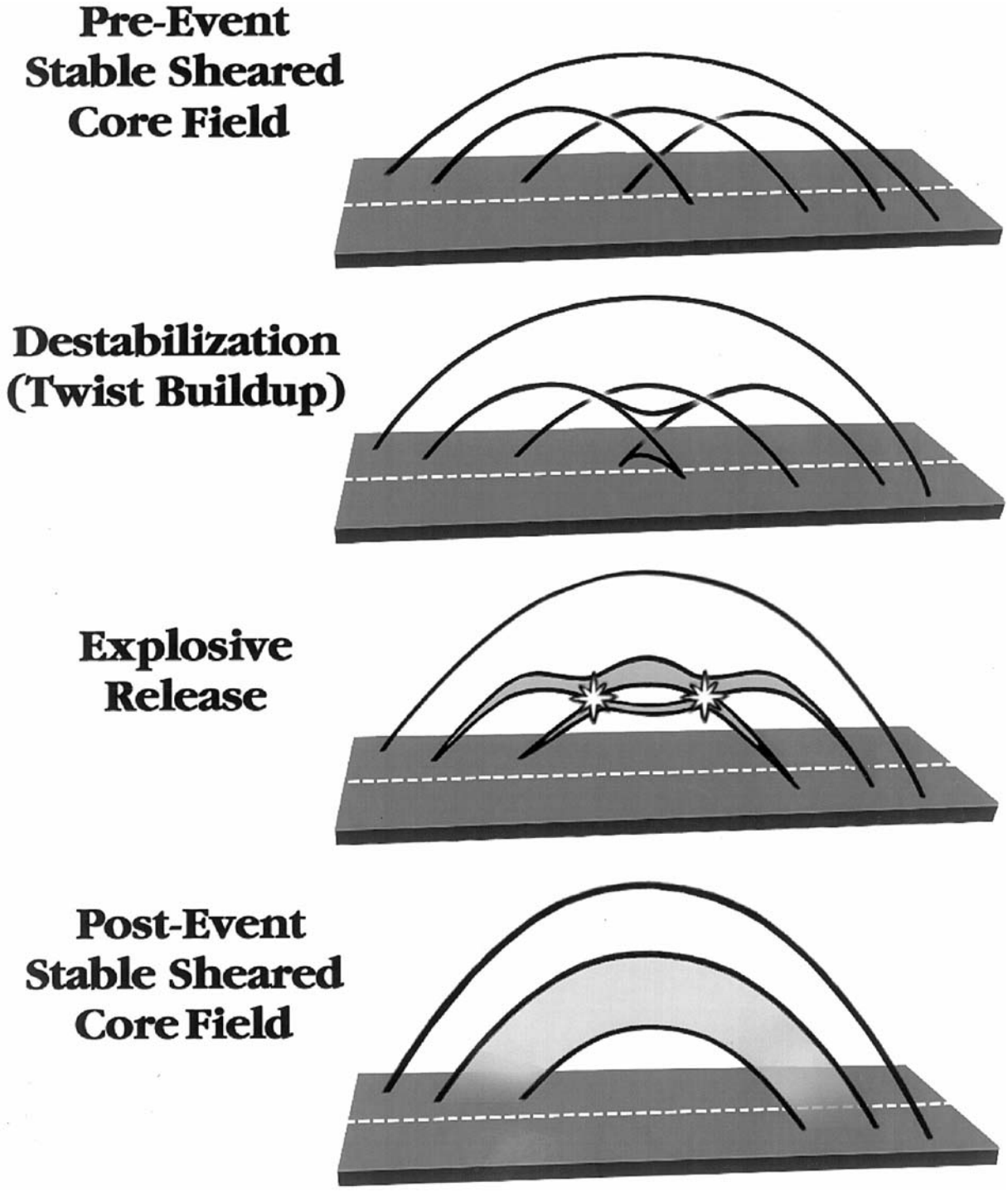

FIG. 3.—Conceptual model for the magnetic explosion that drives a microflare in sheared core field. The heating to X-ray temperatures is assumed to occur via reconnection, which presumably occurs at localized transient sites of intense electric current (large curl ***B***). This suggests that at any instant during the microflare the X-ray plasma might fill only a small fraction of the volume that the microflaring strand appears to have in coronal X-ray images having spatial resolution comparable to the apparent width of the strand. That is, the X-ray plasma might reside in subresolution filaments more or less as depicted in the sketch for the explosive release phase.

sketched in figure 4. This sketch is for a planar cut through the active region; the cut is in the plane of the brightest extended loop (loop C) and intersects both the magnetic island and the main neutral line (the intersection of this plane with the photosphere is a line that passes through the letters F and A in Fig. 1). The sketch shows two micro-explosions in progress, one in the sheared core field on the west side of the magnetic island and the other in the sheared core field on the main neutral line. There is a basic difference in the magnetic environments of these two explosions: the island has a magnetic null over it, whereas the core field at the main neutral line has no such structure near it. We suppose that the magnetic null results in the explosion at the island being more effective in driving external coronal heating. In our concept, both explosions produce some internal heating via internal reconnection and some exter-

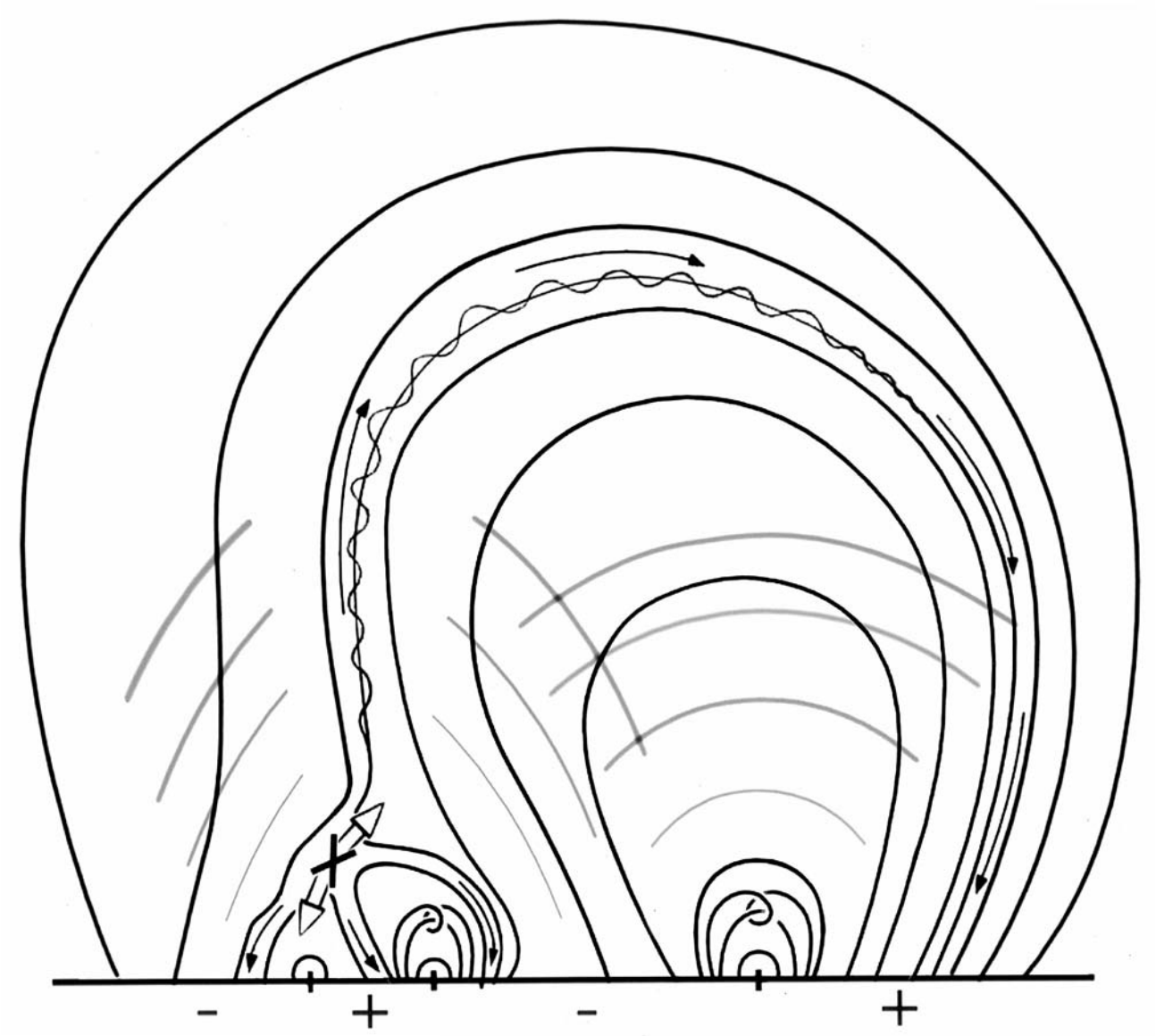

FIG. 4.—Our scenario for the driving of coronal heating by corefield microexplosions in our example active region. The microexplosions drive in situ coronal heating via reconnection as depicted in Fig. 3. The internal convulsion and reconnection of the magnetic field in these confined explosions also generate MHD waves that heat coronal halos around the core fields. The microexplosions in the core field around the magnetic island produce additional remote coronal heating by driving external reconnection at the magnetic null over the island. This reconnection injects MHD disturbances, energetic particles, and hot plasma into extended loops, as in a flaring arch or coronal X-ray jet. The extended loops that receive most of this extra heating are those that have their feet shifted by the reconnection at the null.

nal heating via MHD waves. The internal heating produces an X-ray brightening (microflare) within the core field, while some of the MHD waves reach and heat the halo. However, unlike the explosion at the main neutral line, the explosion at the island, in addition, drives external reconnection at the null. There are two ways for this reconnection to drive coronal heating in the extended loop that stems from the reconnection site. One way is for the reconnection to directly produce energetic particles, hot plasma, and MHD waves that escape into the extended loop as in a flaring arch. The other way is for the reconnection to infuse the extended loop with fine-scale magnetic structure and its concomitant fine-scale electric currents. Production of filamentary currents in an extended loop by reconnection at a magnetic null at the foot of the loop has been demonstrated in numerical simulations by Karpen, Antiochos, & Devore (1996). Much of the coronal heating in the extended loop might be provided by the dissipation of such imposed fine-scale currents.

We now turn to assessing the feasibility of our magnetic microexplosion scenario for supplying the energy for the observed coronal heating in our active region. In subsequent subsections, we will estimate the magnitude of the energy needed for the coronal heating in typical microflaring strands of core field from their size, lifetime, and brightness in the coronal X-ray images. In the remainder of the present subsection, we present the model and formulas that we use to estimate the free magnetic energy content of a strand and the magnitude of the microexplosion needed to supply the heating energy. We suppose that the magnetic energy release in each microflare occurs via expansion and untwisting of the magnetic field of the strand in the manner

sketched in Figure 3. To obtain our estimates, we approximate the exploding field strand model of Figure 3 by the still simpler cylindrical twisted flux tube model of Moore (1988), shown here in Figure 5.

The vector magnetogram in Figure 1 shows that the sheared field in each of the core features A, B, and F was nearly orthogonal to the direction it would have had if it were relaxed to its minimum-energy potential configuration. This means that nearly all of the magnetic energy in these core fields was stored nonpotential magnetic energy that in principle was available for release. So, the free magnetic energy $E_{\rm mag}$ in a microflaring strand in these core fields is approximately its total magnetic energy content:

$$E_{\rm mag} \sim \left(\frac{B^2}{8\pi}\right)\pi r^2 l\,, \tag{1}$$

where $\pi r^2 l$ is the volume of the strand (in our cylindrical flux tube approximation), r and l are the radius and length of the strand, and $B^2/8\pi$ is a representative value for the magnetic energy density in the strand. We will find that the amount of magnetic energy $-\Delta E_{\rm mag}$ needed to be released for a typical microflare is much less than the total stored magnetic energy in the strand: $-\Delta E_{\rm mag} \ll E_{\rm mag}$. This implies that only a small expansion and/or untwisting of the field strand is needed to release the energy for a microflare. By using the cylindrical twisted flux tube model of Moore (1988) as follows, we can estimate to order of magnitude the small changes in the strand width and twist needed for a given small energy release.

Even though in any actual microexplosion of a twisted field strand, the magnetic energy decrease results partly from expansion of the field and partly from untwisting of the field via reconnection (as in Fig. 3), for rough estimates of the amount of expansion or untwisting needed for a microflare, we may consider two extreme cases: the case in which the magnetic energy decreases by expansion alone, and the opposite extreme in which there is no expansion and the magnetic energy is released by untwisting alone. The magnetic field in the model flux tube is composed of two orthogonal components, parallel and perpendicular to the axis of the tube:

$$\boldsymbol{B} = \boldsymbol{B}_{\parallel} + \boldsymbol{B}_{\perp}\,, \tag{2}$$

so that

$$B^2 = B_{\parallel}^2 + B_{\perp}^2\,. \tag{3}$$

The magnetic energy content of the flux tube has two corresponding parts:

$$E_{\rm mag} = E_{\rm mag\parallel} + E_{\rm mag\perp}\,, \tag{4}$$

where

$$E_{\rm mag\parallel} \sim \frac{B_{\parallel}^2}{8\pi}\,\pi r^2 l \tag{5}$$

and

$$E_{\rm mag\perp} \sim \frac{B_{\perp}^2}{8\pi}\,\pi r^2 l\,. \tag{6}$$

In these approximate equations for $E_{\rm mag\parallel}$ and $E_{\rm mag\perp}$, $B_{\parallel}$ and $B_{\perp}$ are representative values for these field components in the flux tube. Now, for an estimate of the amount of expansion needed for a given amount of energy release, we take the expansion of the flux tube to be mostly lateral, so that the fractional increase in the length of the flux tube is negligible compared to the fractional increase in the diameter. This approximation seems reasonable for the majority of core-field microflares in our active region because they appear not to be ejective but to be well confined, more or less as in Figure 3. In this approximation, in the case of energy release by expansion alone, there is negligible change in the perpendicular magnetic energy compared to the change in the parallel magnetic energy, and, for small expansion, the fractional decrease in the parallel magnetic energy is twice the fractional increase in the tube diameter d:

$$\frac{\Delta E_{\rm mag\parallel}}{E_{\rm mag\parallel}} \sim -2\,\frac{\Delta d}{d}\,. \tag{7}$$

For the opposite extreme of energy release by untwisting alone, the parallel magnetic energy remains constant, and,

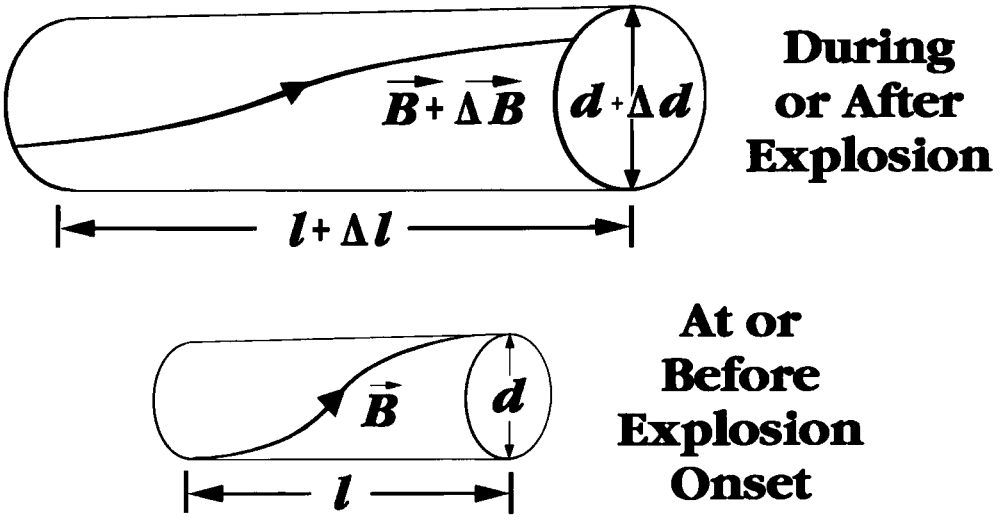

FIG. 5.—The cylindrical twisted flux tube model used for estimating the magnetic energy content of a microflaring strand of sheared core field and the amount of expansion and/or untwisting needed to release enough energy for the microflare. (Modified from Moore 1988).

for small decreases in twist, the fractional decrease in the perpendicular magnetic energy is twice the fractional decrease in the perpendicular field strength:

$$\frac{\Delta E_{\mathrm{mag}\perp}}{E_{\mathrm{mag}\perp}} \sim 2\,\frac{\Delta B_{\perp}}{B_{\perp}}\,. \tag{8}$$

3.3. *Directly Measured Quantities for Elements of the Coronal X-Ray Features in Our Active Region*

Our next step is to single out three representative elementary coronal structures in our active region for quantitative analysis of the coronal heating energetics. We take all of the core features in Figures 1 and 2 to be composed of microflaring strands of core field, with several strands overlapping along the line of sight in the brighter parts. For application of our exploding strand model, we have selected two core structures that in Figure 2 appear to be individual strands. One is at the south end of core feature A on the main neutral line, and the other is on the south side of core feature F at the magnetic island. The strand on the main neutral line undergoes a microflare brightening in the 5 minute interval covered by the bottom row of three frames in Figure 2, and the strand at the island microflares in the 5 minute interval of the next row up. In Figure 2 it appears that at any instant a few tens of such microflares are in progress along the main neutral line and a few ($\sim$3) are in progress in core feature F at the foot of the bright extended loop (loop C). In our picture, the microexplosions in the core field along the main neutral line drive the coronal heating there, and the microexplosions in the core field at the foot of the bright extended loop drive both the heating in this core field and the heating in the extended loop. So, the third coronal structure for which we will quantify the energetics of the heating is bright loop C.

For each of our three selected coronal features, the quantities that can be directly measured or estimated from the coronal images of Figure 2 are the diameter and length of the strand or loop, the X-ray brightness, and (for our two microflares) the lifetime. We estimate the lifetime of loop C from Figure 9 of Falconer et al. (1997), which shows the evolution of the extended loops over a span of four hours beginning with the orbit of our Figures 1 and 2. We estimate the magnetic field strength in our two microflaring strands from the vector magnetogram in Figure 1. The twist in the core field on the main neutral line is estimated from the apparent twist seen in the coronal core features there in Figure 2, and we assume that the twist in the microflaring strand at the island is of the same order. The adopted values for these directly obtained empirical quantities are listed in Table 1. The uncertainty in each entry is roughly a factor of two. All three of our features had about the same brightness. The two microflare strands were of the same diameter but different length, the one at the island being shorter. Each microflare lasted for about 5 minutes, whereas the much larger bright extended loop lasted for 2–3 hr. From a study of hundreds of microflares in active regions observed by the *Yohkoh* SXT, Shimizu (1995) found that most microflares have sizes, shapes, brightnesses, and durations of the order of those of our two selected microflares. That is, our two microflares are typical of the microflares observed in active regions by the *Yohkoh* SXT.

3.4. *Derived Thermal Energetic Quantities*

From the quantities in Table 1, we now proceed to estimate the energy required to sustain the coronal heating in each of our selected features over its lifetime. Two physical quantities entering into these estimates are the temperature and density of the X-ray emitting plasma. The density is determined by the X-ray brightness, the temperature, and the fraction of the volume of the feature filled by the X-ray plasma. This volume fraction, the so-called filling factor, is important in that the heating energy is proportional to it.

From filter-pair intensity ratios, Shimizu (1995) found the temperature of the X-ray plasma in most microflares to be in the range 4–8 MK. Similarly, Yoshida & Tsuneta (1996) found that active-region loops like our bright extended loop that have lifetimes of no more than a few hours usually have temperatures in the range 5–8 MK. So, for our energy estimates, we adopt 6×10^6 K for the X-ray plasma temperature in each of our three features. For plasma temperatures in the range 3–10 MK, the plasma density and the brightness of a feature are related as follows for SXT images taken with the thin aluminum filter (Tsuneta et al. 1991):

$$\langle n_e^2 \rangle = 10^{25}\,\frac{I}{d}\,\mathrm{cm}^{-6}\,, \tag{9}$$

where I (DN s^{-1} pixel^{-1}) is the brightness, d (cm) is the diameter of the strand or loop along the line of sight, and $\langle n_e^2 \rangle$ is the mean square of the electron density along d. The density given by $\langle n_e^2 \rangle^{1/2}$ is a lower bound on the actual density; it equals the actual density only if the strand or loop is uniformly full of plasma of this density. If the loop is

TABLE 1

DIRECTLY MEASURED QUANTITIES FOR ELEMENTS OF THE CORONAL X-RAY FEATURES IN OUR ACTIVE REGION

	FEATURE		
QUANTITY	Typical Microflaring Strand of Core Field on Main Neutral Line	Typical Microflaring Strand of Core Field at Foot of Bright Extended Loop	Bright Extended Loop
Diameter d (cm)	3×10^8	3×10^8	1×10^9
Length l (cm)	1.5×10^9	1×10^9	1.5×10^{10}
Brightness I (Dn s^{-1} pixel^{-1})	4×10^3	4×10^3	4×10^3
Lifetime τ_{feature} (s)	3×10^2	3×10^2	1×10^4
Total magnetic field $B(G)$	5×10^2	5×10^2	...
Axial component $B_{\parallel}(G)$	5×10^2	5×10^2	...
Azimuthal component $B_{\perp}(G)$	2×10^2	2×10^2	...

only partially filled by filaments of density n_e, then in order for the loop to have its observed brightness, the filling factor f (the fraction of the volume of the loop filled by the plasma filaments) is the ratio of the mean square density through the loop to the square of the actual density in the filaments. Thus, $\langle n_e^2 \rangle^{1/2}$ is less than the actual density by the square root of the filling factor:

$$n_e = \langle n_e^2 \rangle^{1/2} f^{-1/2} . \quad (10)$$

A physically reasonable upper bound on the density in the X-ray plasma filaments within a loop is the density n_e^* at which radiation and conduction contribute equally to the cooling of the plasma. The rate of energy loss by radiation per unit volume is $\Lambda_r n_e^2$, where the radiative cooling coefficient Λ_r is a function of temperature determined by the elemental composition of the plasma. For coronal abundances, Λ_r is roughly constant $\sim 3 \times 10^{-23}$ ergs cm^3 s^{-1} in the temperature range 3–10 MK (Cook et al. 1989). The rate of energy loss by conduction per unit volume is the divergence of the heat flux flowing out of the X-ray plasma to the cooler plasma at the feet of the loop. For a filament of length l, the divergence of the heat flux in the X-ray plasma is given to order of magnitude by $\kappa_c T/(l/2)^2$, where κ_c is the thermal conductivity. To a good approximation the thermal conductivity in the corona is a function of temperature alone: $\kappa_c = 10^{-6} T^{5/2}$ ergs cm^{-1} s^{-1} K^{-1} (Spitzer 1962). Equating the radiative and conductive loss rates gives

$$n_e^* \sim \frac{5 \times 10^8 T^{7/4}}{l} \text{ cm}^{-3} . \quad (11)$$

Thus, n_e^* is determined by the temperature of the X-ray plasma and the length of the loop. As discussed by Moore et al. (1980) for the thermal X-ray plasma in flares, if the density in a plasma filament is less than n_e^*, then conductive cooling dominates over radiative cooling and the conductive heat flux goes mainly into driving chromospheric evaporation, which increases the plasma density in the hot filament. If each filament is (1) heated transiently for less than the conductive cooling time, as seems reasonable in our microflare reconnection scenario (Figs. 3 and 4), and (2) initially has some $n_e < n_e^*$, then the density should not increase much beyond n_e^*. For at densities beyond n_e^*, radiative cooling would dominate over conductive cooling and the plasma would cool below X-ray–emitting temperatures before conduction could produce any large further increase in the density. We therefore take n_e^* as a reasonable approximate upper bound on the X-ray plasma density in our selected coronal features. This limits the filling factor to the range above $\langle n_e^2 \rangle / n_e^{*2}$:

$$\frac{\langle n_e^2 \rangle}{n_e^{*2}} \lesssim f \leq 1 . \quad (12)$$

To order of magnitude, the thermal energy content E_{th} of the X-ray plasma in any one of our three coronal features at any instant is the thermal energy density ($3 n_e kT = 3 \langle n_e^2 \rangle^{1/2} f^{-1/2} kT$) times the volume of the X-ray plasma in the feature (fV):

$$E_{\text{th}} \sim \langle E_{\text{th}} \rangle f^{1/2} , \quad (13)$$

where, $\langle E_{\text{th}} \rangle = 3 \langle n_e^2 \rangle^{1/2} kTV$ and $V \sim \pi (d/2)^2 l$. Thus, $\langle E_{\text{th}} \rangle$ is the maximum possible thermal energy content. For densities $\lesssim n_e^*$, the cooling time τ_{cooling} for the X-ray plasma is of the order of the conductive cooling time τ_c given by the thermal energy density divided by the divergence of the heat flux:

$$\tau_{\text{cooling}} \sim \langle \tau_c \rangle f^{-1/2} , \quad (14)$$

where $\langle \tau_c \rangle = 3 \langle n_e^2 \rangle^{1/2} kT [\kappa_c T/(l/2)^2]$. Smaller filling factors give longer cooling times. As we will see, for each of our three selected coronal features we may assume that the cooling time is shorter than the observed lifetime of the feature. This condition requires that the coronal heating rate $(dE/dt)_{\text{heating}}$ roughly equal the cooling rate in each feature:

$$(dE/dt)_{\text{heating}} \sim E_{\text{th}}/\tau_{\text{cooling}} \sim \langle (dE/dt)_{\text{heating}} \rangle f , \quad (15)$$

where $\langle (dE/dt)_{\text{heating}} \rangle = \langle E_{\text{th}} \rangle / \langle \tau_c \rangle$. The area-average energy flux F_{heating} for supplying the coronal heating in any one of our coronal features is the heating rate divided by an appropriate area A_{feature}:

$$F_{\text{heating}} \sim \langle F_{\text{heating}} \rangle f , \quad (16)$$

where $\langle F_{\text{heating}} \rangle = \langle (dE/dt)_{\text{heating}} \rangle / A_{\text{feature}}$. For our two core-field strands we take A_{feature} to be the spanned area (ld), but for the bright extended loop take A_{feature} to be the end area ($\pi d^2/4$) because we suppose that this loop's heating energy comes up from its end at the island. Finally, the total coronal heating energy E_{heating} spent on a feature during its life is the heating rate times the feature's lifetime τ_{feature}:

$$E_{\text{heating}} \sim \langle (dE/dt)_{\text{heating}} \rangle f \tau_{\text{feature}} . \quad (17)$$

Thus, the heating rate, the heating energy flux, and the lifetime heating energy are all proportional to the filling factor.

For each of our three coronal features, from the values of quantities in Table 1 and the temperature, we can estimate each of the thermal energetic quantities given by equations (9)–(17). These estimates are listed in Table 2. As should be expected, the upper and lower bounds on the density given in Table 2 show that the density is probably greater in the low-lying core-field microflares than in the much higher-reaching extended loop. Table 2 also shows that the thermal energy produced in each of the two microflares is about the same, as we would expect from the similarity of these two features in Figure 2. Because of its larger size and similar brightness, the bright extended loop has (1) a thermal energy content much larger than that of the core-field microflares (provided that the filling factor is not vastly smaller in the extended loop than in the microflares) and (2) a much longer cooling time than that of the core field microflares (provided that the filling factor is not vastly larger in the extended loop than in the microflares). These two counter-acting differences result in the heating rate for the extended loop being comparable to the heating rate in the representative microflare at its base. If, as appears to be so in Figure 2, roughly three such microflares are in progress at the foot of the extended loop at any instant, the energy for the heating in the extended loop can be supplied by these microflares if each microflare feeds about a third as much energy into the extended loop as goes to the microflare's internal coronal heating. Thus it appears that these microflares are similar to larger flares in active bipoles that drive flaring-arch heating in impacted larger passive loops: the internal coronal heating driven in the flaring bipole is greater than the remote coronal heating driven in the

TABLE 2

DERIVED THERMAL ENERGETIC QUANTITIES FOR ELEMENTS OF THE CORONAL X-RAY FEATURES IN OUR ACTIVE REGION

QUANTITY	FEATURE		
	Typical Microflaring Strand of Core Field on Main Neutral Line	Typical Microflaring Strand of Core Field at Foot of Bright Extended Loop	Bright Extended Loop
Temperature T (K)	6×10^6	6×10^6	6×10^6
Density Lower Bound $\langle n_e^2 \rangle^{1/2}$ (cm^{-3})	1×10^{10}	1×10^{10}	6×10^9
Density upper bound n_e^* (cm^{-3})	2.5×10^{11}	4×10^{11}	2.5×10^{10}
Filling factor f	$\gtrsim 1.5 \times 10^{-3}$	$\gtrsim 6 \times 10^{-4}$	$\gtrsim 6 \times 10^{-2}$
Density n_e (cm^{-3})	$10^{10} f^{-1/2}$	$10^{10} f^{-1/2}$	$6 \times 10^9 f^{-1/2}$
Thermal energy content $E_{\rm th}$ (ergs)	$3 \times 10^{27} f^{1/2}$	$2 \times 10^{27} f^{1/2}$	$2 \times 10^{29} f^{1/2}$
Cooling time $\tau_{\rm cooling}$ (s)	$2.5 \times 10 f^{-1/2}$	$10 f^{-1/2}$	$1.5 \times 10^3 f^{-1/2}$
Heating rate $(dE/dt)_{\rm heating}$ (ergs s)	$10^{26} f$	$2 \times 10^{26} f$	$1.5 \times 10^{26} f$
Heating energy flux $F_{\rm heating}$ (ergs cm^{-2} s^{-1})	$2.5 \times 10^8 f$	$6 \times 10^8 f$	$1.5 \times 10^8 f$
Lifetime heating energy $E_{\rm heating}$ (ergs)	$3 \times 10^{28} f$	$6 \times 10^{28} f$	$1.5 \times 10^{30} f$

extended loop. That is, our estimates in Table 2 indicate that the core-field microflares at the foot of the bright extended loop follow the first two rules for flare heating stated at the end of § 2.

Now consider the heating energy fluxes in Table 2. On the basis of empirical estimates from measurements of the solar wind and from EUV and X-ray observations of the solar atmosphere, it is generally accepted that the energy flux to sustain the corona and solar wind from quiet regions is no less than several times 10^5 ergs cm^{-2} s^{-1} and that the average energy flux for coronal heating in active regions is at least an order of magnitude greater, $\sim 10^7$ ergs cm^{-2} s^{-1} (Withbroe & Noyes 1977; Withbroe 1988). Our selected coronal features are among the brightest ones in our active region. Hence, it is unlikely that $F_{\rm heating}$ is less than 10^7 ergs cm^{-2} s^{-1} in our features. With this empirical limit, it appears from our estimates of $F_{\rm heating}$ in Table 2 that 10^{-2} is a strong lower bound on the filling factor in each of our three features. This verifies that the actual density in our features is $\lesssim n_e^*$ (which upper bound we expected from physical reasoning) and confirms that the cooling time should be approximately the conductive cooling time. For $n_e \lesssim n_e^*$, the cooling time for each feature in Table 2 is less than the observed lifetime, justifying our assumption that the heating time is comparable to the cooling time. While the heating energy flux requires the filling factor in our features to be well above 10^{-2}, we still expect the filling factor to be well below unity both because the diameters of our microflare strands are at the limit of resolution of the SXT images and because we expect that the heating in our features is driven via reconnection, an inherently fine-scale process. Furthermore, for each of our three features, by comparing the conductive cooling time in Table 2 with the lifetime in Table 1, we can deduce that the filling factor cannot be near unity. For if the filling factor were unity, then the conductive cooling time would be ~ 10 times shorter than the lifetime, and the conductive heat flow to the feet would increase the density of the $\sim 6 \times 10^6$ K plasma and hence the X-ray brightness of the feature many fold over the lifetime of the feature, in contradiction to the observed lack of such an increase in brightness. (For filling factors much less than unity, there is room within the feature for the heating to pass through a sequence of subfilaments, each subfilament filling a small fraction of the volume of the whole feature and each remaining at coronal X-ray temperatures for a short time in the whole life of the feature. This permits a density history of the X-ray plasma in the feature that is compatible with the observed brightness history.) So, in our two selected microflares, and in our selected extended loop as well, we conclude that f must be much smaller than 1 and much larger than 10^{-2}. Therefore, we adopt 10^{-1} as a reasonable order-of-magnitude working value for the filling factor in each of our three features.

If each microflare at the foot of the bright extended loop injects a third of the heating energy needed to sustain the X-ray plasma in the extended loop during the microflare's 300s life, then each microflare injects $\sim 1.5 \times 10^{28} f$ ergs into the extended loop, where f is the filling factor in the extended loop. In comparison, the thermal energy content of the extended loop is $\sim 2 \times 10^{29} f^{1/2}$ ergs. That is, for $f \sim 10^{-1}$, the injected energy needed from each microflare is only a few percent of the thermal energy of the X-ray plasma in the extended loop. So, even though in Figure 2 the extended loop shows no obvious changes on the time scale of the microflares, it is still reasonable for the heating in the extended loop to be driven by the microflaring activity in the core field at its foot.

3.5. *Derived Magnetic Energetic Quantities*

As we discussed above, the thermal energetic estimates in Table 2 show that if magnetic microexplosions can sustain the coronal heating in the sheared core fields in our active region, then these microexplosions in the core field at the foot of the bright extended loop can plausibly also drive the coronal heating in the extended loop. With the lifetime heating energy in hand for our two core-field microflares, we can now turn to the question of whether the sheared core fields have enough stored magnetic energy to supply the observed persistent strong coronal heating in our active region, as well as the question of the magnitude of a typical microexplosion in terms of the expansion and/or untwisting of the magnetic strand.

For each of our two core-field microflare strands, the magnetic energetic quantities of interest are $E_{\rm mag}$, the stored magnetic energy in the strand; $N_{\rm stored}$, the number of microflares to deplete $E_{\rm mag}$; $\tau_{\rm depletion}$, the time span in which $N_{\rm stored}$ microflares occur in the strand; $\Delta d/d$, the fractional lateral expansion of the strand field to fuel one microflare; and $\Delta B_\perp / B_\perp$, the fractional decrease in $B_\perp$ to fuel one microflare by untwisting of the strand field. $E_{\rm mag}$ is given by

equation (1) with values of B, $r(=d/2)$, and l from Table 1. We estimate $N_{\rm stored}$ for each strand by

$$N_{\rm stored} \sim \langle N_{\rm stored} \rangle f^{-1} , \quad (18)$$

where $\langle N_{\rm stored} \rangle = E_{\rm mag}/\langle E_{\rm heating} \rangle$. The depletion time is inversely proportional to the frequency of microflares in the strand. From inspection of Figure 2, we estimate that in each of our two strands a microflare was occurring about a third of the time. With this approximation, the depletion time is estimated by

$$\tau_{\rm depletion} \sim \langle \tau_{\rm depletion} \rangle f^{-1} , \quad (19)$$

where $\langle \tau_{\rm depletion} \rangle = 3\tau_{\rm feature} \langle N_{\rm stored} \rangle = 900 \langle N_{\rm stored} \rangle$ s. The fractional lateral expansion to fuel a microflare is given by equation (7), with $\Delta E_{\rm mag\parallel} = -E_{\rm heating}$. Likewise, the fractional decrease in $B_\perp$ to fuel a microflare by untwisting of the field is given by equation (8), with $\Delta E_{\rm mag\perp} = -E_{\rm heating}$.

For each of our two microflaring strands, our estimates of the five magnetic energetic quantities are listed in Table 3. For $f \sim 10^{-1}$, $N_{\rm stored}$ is $\gtrsim 100$ and the depletion time is $\gtrsim 1$ day for either strand. The estimates of $\tau_{\rm depletion}$ in Table 3 indicate that the sheared core field along the main neutral line had enough stored energy to sustain the intense coronal heating there for more than a day, and that the sheared core field at the base of the bright extended loop could fuel the coronal heating in itself and in the extended loop for about a day. A day is a typical timescale for substantial evolutionary changes in the total magnetic flux, large-scale magnetic configuration, and neutral-line magnetic shear in active regions (e.g., Moore & Rabin 1985). So it is plausible that the nonpotential energy in the core fields could build up as fast or faster than it needed to be depleted by the microflaring. Thus, our core-field microexplosion scenario for coronal heating is feasible in our active region in terms of the stored energy in the sheared core fields and the required rate of depletion of this energy.

For $f \sim 10^{-1}$, the required lateral expansion or untwisting of the microflaring field strand is no greater than a few percent for a typical microflare in either of our two strands. That is, any combination of expansion and untwisting that releases $\lesssim 10^{28}$ ergs in one of our microflaring flux tubes, produces only a slight change in the diameter and twist of the flux tube. Thus, the character of most of the magnetic microexplosions needed for the coronal heating in our active region is that of confined tremors in the core fields rather than that of full-blown explosions.

The first frame of Figure 2 shows, in the core field at the foot of extended loop D, a heating event that was larger and much stronger than either of our selected representative microflares. It was strong enough to saturate the SXT coronal image and large enough to be seen as a subflare in ground-based chomospheric images (Porter et al. 1994). A typical subflare releases $\sim 10^{29}$ erg (Svestka 1976). In our model, this amount of energy would be released by a $\sim 10\%$ expansion and/or untwisting of a strand of the size and field strength of our two representative strands, or by a $\sim 1\%$ expansion/untwisting of a strand having a volume an order of magnitude larger than our selected strands. An energy-release event of this magnitude at the foot of either of the extended loops in our active region should produce a noticeable brightening in the extended loop if it feeds $\sim 1/3$ of its energy into the extended loop. The strong core-field event in Figure 2 probably did make extended loop D brighten by $\gtrsim 25\%$ because this loop gradually dimmed by about 25% over the 50 minute span of Figure 2 (Porter et al. 1994).

In summary, the thermal and magnetic energetic estimates in Tables 2and 3 show that it is quite feasible for the persistent coronal heating in our active region—and the subflare as well—to be powered by magnetic microexplosions in the core fields. Thus, in addition to fitting the first two rules for flare heating stated in § 2, it is also feasible for core-field microflaring in our active region to follow the third rule: the coronal heating in core fields and in the extended loops can be driven by eruptive magnetic action in the sheared core fields.

4. SUMMARY AND PROSPECTS FOR CORONAL HEATING IN QUIET REGIONS AND CORONAL HOLES

By combining *Yohkoh* SXT coronal X-ray images and MSFC vector magnetograms, Falconer et al. (1997) examined the magnetic locations of outstanding bright coronal X-ray features in active regions. They found that nearly all of these strongly heated magnetic structures were rooted near neutral lines, each feature being either a core feature embedded within the core field low along a neutral line or an extended loop stemming from close around the core field, or a combination of these two elements. Moreover, the large majority of the core fields at these sites of strong coronal heating were found to be strongly sheared and the bright core features within them to be continually microflaring, i.e., they continually underwent fine-scale changes in brightness and structure on few-minute timescales. In the present paper, we have pointed out that most if not all flares are also seated on neutral lines with strongly sheared core fields, that the intense heating in these flares is apparently magnetically driven by explosive eruption of the shared core field, and that in addition to driving intense coronal

TABLE 3

DERIVED MAGNETIC ENERGETIC QUANTITIES FOR TYPICAL CORE-FIELD MICROFLARES IN OUR ACTIVE REGION

	FEATURE	
QUANTITY	Microflaring Strand of Sheared Core Field on Main Neutral Line	Microflaring Strand of Sheared Core Field at Foot of Bright Extended Loop
Stored magnetic energy $E_{\rm mag}$ (ergs)	10^{30}	8×10^{29}
Number of microflares to deplete $E_{\rm mag} N_{\rm stored}$	$30f^{-1}$	$10f^{-1}$
Depletion time $\tau_{\rm depletion}$ (s)	$3 \times 10^4 f^{-1}$	$10^4 f^{-1}$
Lateral expansion to drive one microflare $\Delta d/d$	$1.5 \times 10^{-2} f$	$4 \times 10^{-2} f$
Untwisting to drive one microflare $-\Delta B_\perp/B_\perp$	$10^{-1} f$	$2.5 \times 10^{-1} f$

heating within itself, the exploding core field often drives strong heating in larger passive magnetic loops that have one end impacted against the sheared-core bipole. This suggests that the quasi-steady persistent strong coronal heating in active regions is magnetically driven in basically the same way as the transient intense coronal heating in flares, with the driving being done by a staccato of localized microexplosions in the sheared core fields rather than the global explosion that drives a full-sized flare.

In this paper, we have developed our core-field microexplosion scenario for coronal heating enough to test its energetic feasibility in an example active region from the set studied by Falconer et al. (1997). Our estimates of the stored magnetic energy in microflaring strands of core field together with estimates of the energy spent on coronal heating in typical microflares and in a bright extended loop show that our scenario is indeed feasible for the coronal heating in this active region. These energy estimates in combination with a simple twisted flux tube model for the microflaring strands yield the following conclusions:

1. The filling factor for the $\sim 6 \times 10^6$ K X-ray–emitting plasma in the brighter coronal features in *Yohkoh* SXT images of our active region was $\sim 10^{-1}$. This means that the density of the X-ray plasma was ~ 3 times greater and the heating energy to sustain this hot plasma was ~ 10 times smaller than for a filling factor of unity.

2. The X-ray plasma density was $\sim 3 \times 10^{10}$ cm^{-3} in the microflaring strands in the core field and ~ 2 times less in the bright extended loop. Because these densities are less than that at which radiative cooling would be as strong as conductive cooling, the X-ray plasma was cooled mostly by heat conduction.

3. Because the thermal energy content of the bright extended loop was ~ 100 times the energy released in a typical microflare at its foot, the heating in the extended loop could have been sustained by energy injections from these microflare events even though the extended loop showed no noticeable X-ray brightness variations on timescales of the microflares.

4. The core fields in our active region had enough stored magnetic energy to supply the observed coronal heating for a day or more, a time of the order of that typical for the buildup of sheared core fields in active regions.

5. The typical magnetic microexplosion driving the coronal heating in the observed microflares and extended loops need produce only a slight ($\sim 1\%$) expansion and/or untwisting of the microflaring field strand to release enough magnetic energy.

6. The observed coronal heating can be produced by sheared core field microflare events that follow analogs of our three empirical rules for the heating in full-sized core-field flares: (1) the strongest heating is driven within a microflaring strand of core field; (2) somewhat less heating is driven in extended loops rooted against the sheared core field; (3) both the internal heating and the external heating are driven by explosive action of the magnetic field in the microflaring strand.

The study of strong coronal heating in active regions by Falconer et al. (1997) sampled five active regions, enough to show that much of the strong coronal heating in active regions is directly connected with strongly sheared core fields, and that the coronal heating in our example active region is representative of the coronal heating in many active regions. Hence, we infer that the two types of magnetic settings (sketched in Fig. 4) for the two core fields in our example active region are found in many active regions and that our core-field microexplosions scenario is feasible for the coronal heating in and around all such magnetic structures in active regions. In any case, our example active region shows that there are two different magnetic configurations in which a microflaring sheared core field can reside and may reasonably drive the coronal heating within itself and in fields rooted nearby. One is the closed-bipole configuration over the main neutral line, and the other is the more open configuration encompassing the magnetic null over the island of included polarity. The magnetic configuration in and around the sheared core field along the main neutral line is basically that for a single-bipole confined flare (Fig. 6, *upper left*), and the configuration in and around the sheared core field at the magnetic island is basically that of a flaring arch (Fig. 6, *lower right*). Our analysis of the coronal heating energetics in our example active region shows that it is feasible for the driving of the quasi-steady strong coronal heating in these two field configurations to be basically similar to the driving of the burst of heating in full-fledged flares in these fields configurations. This demonstrates the broad idea espoused in the § 1: the configuration of the field holds basic clues to the origins of the coronal heating within it.

We now turn to the relevance of our results on the strong coronal heating in active regions to the weaker but pervasive coronal heating in quiet regions and coronal holes, including the heating that sustains the extended corona and generates the solar wind. Except in and near sunspots in active regions, everywhere on the Sun the magnetic flux is concentrated in a network of lanes and clumps along the edges of the supergranular convection cells. The lanes and clumps are typically 5,000–10,000 km wide, and the cells outlined by the flux concentrations are typically about 30,000 km in diameter. While some lanes and clumps are predominantly of one polarity, nearly all show at least some inclusions of opposite polarity flux in magnetograms with spatial resolution of a few thousand km or better and sensitivity of $\lesssim 10$ G (Harvey 1977; Falconer et al. 1998). The fine-scale mix of opposite polarity flux is produced and maintained by continual addition of new fine-scale flux of both polarities that emerges in the cell interiors and is swept into the network lanes by the supergranular flow (Wang et al. 1996; Schrijver et al. 1997). Consequently, the network lanes are filled by a mixture of two three-dimensional magnetic structures of disparate scale, as sketched in Figure 7: (1) funnels that are the feet of the large scale magnetic loops or open fields that fill the quiet corona and coronal holes, and (2) small closed bipoles packed between and against the feet of the funnels (Dowdy, Rabin, & Moore 1986; Porter & Moore 1988). That is, the network magnetic flux is riddled with neutral lines, each of which is encased in the core field of a small closed bipole.

Depending on the location and orientation of any given network bipole, the magnetic configuration can be either basically that of the magnetic island in our example active region or that of the core field on the main neutral line, the two core-field configurations sketched in Figure 4. Because present vector magnetograms lack the required sensitivity and spatial resolution to map the network core fields, it is unknown whether many or any of the network core fields are strongly sheared. However, it is known that microflare

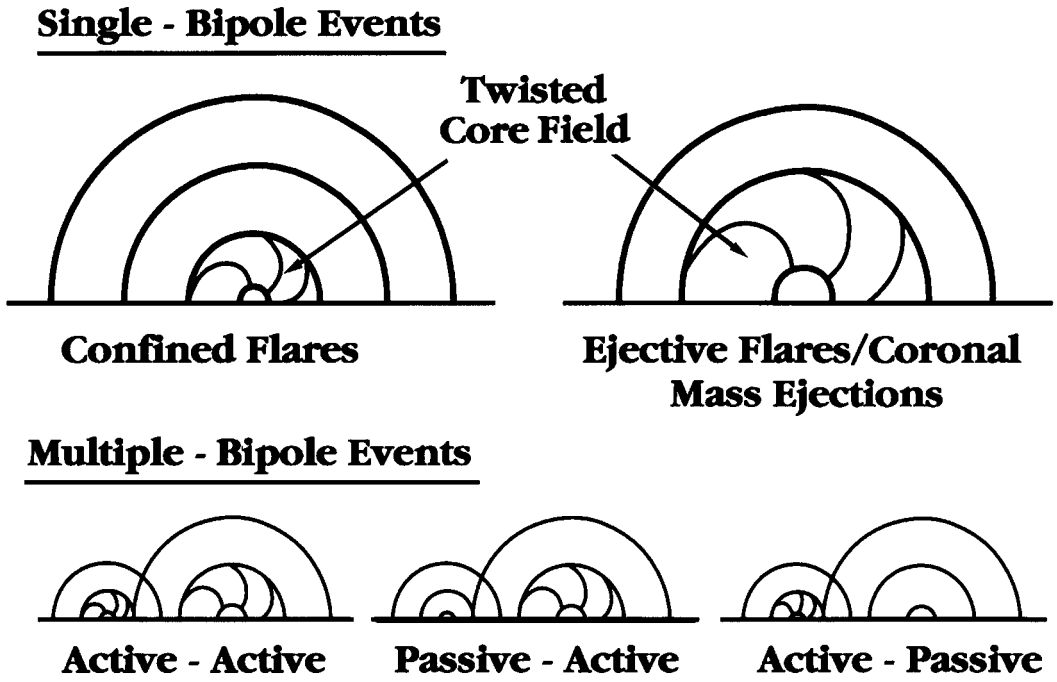

FIG. 6.—Schematic representation of the elementary components of the pre-event magnetic field configurations of flares and coronal mass ejections. Each flare and/or coronal mass ejection arises in a magnetic field configuration that is essentially one or some combination of these elementary configurations. The field configuration determines whether an event (driven by eruptive action of sheared/twisted core fields) produces only a flare or both a flare and a coronal mass ejection and, if both, the relation between the two (see text). (Based on Machado et al. 1988a).

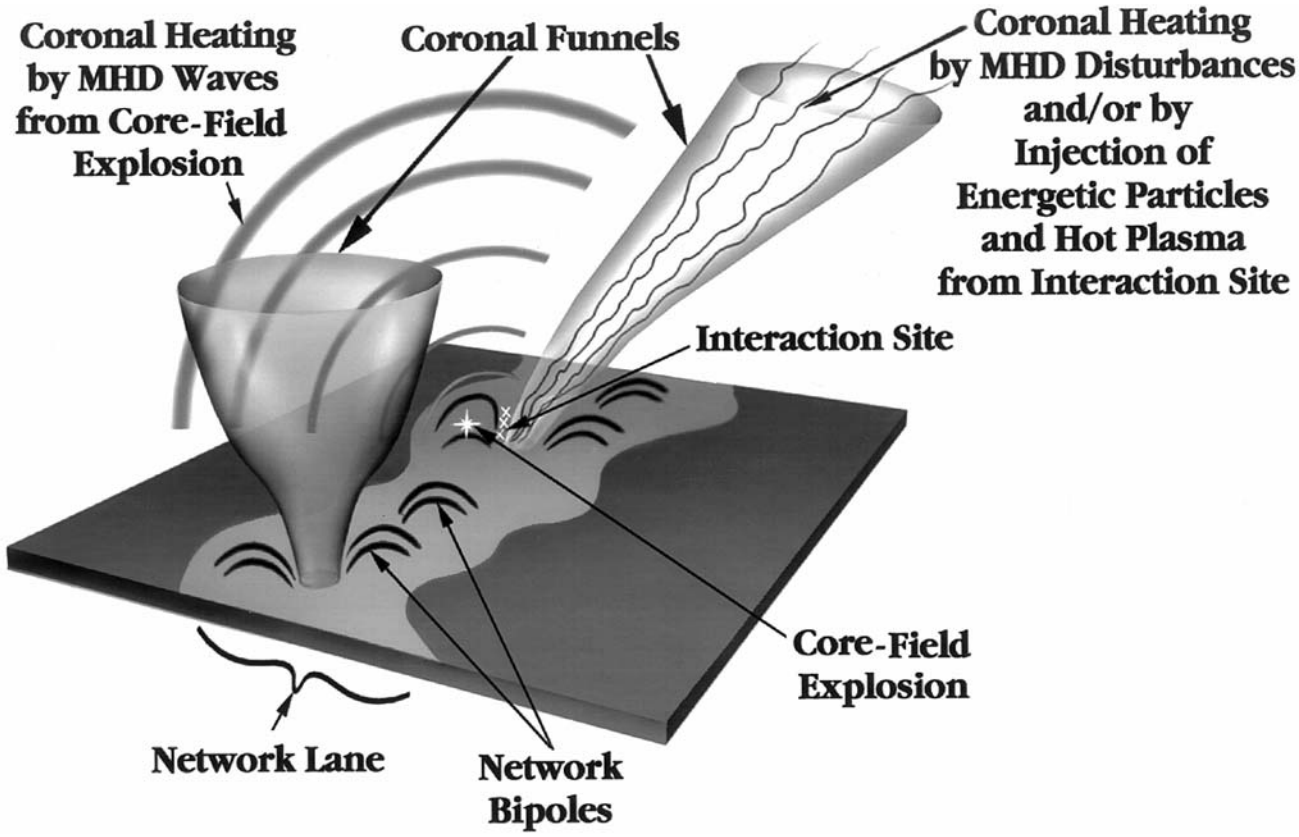

FIG. 7.—Our scenario for heating the corona in quiet regions and coronal holes by core-field explosions in network bipoles. These bipoles are concentrated in and around the network magnetic flux concentrations, and so many are embedded in or impacted against the feet of coronal magnetic funnels, giving a combined field configuration like that of a flaring arch or coronal X-ray jet: an active bipole impacted in one end of a much larger passive magnetic arch or funnel. (Modified from Porter & Moore 1988).

brightenings and explosive turbulent events and jets in transition-region ($\sim 10^5$ K) emission lines frequently occur in network bipoles (e.g., Porter et al. 1987; Porter & Dere 1991), and it was recently found that many network bipoles are heated to coronal temperatures strongly enough to show as faint coronal bright points in XUV coronal images having subnetwork resolution (Falconer et al. 1998). So it is known that many network core fields are seats of microflaring and concentrated coronal heating. On this basis, by analogy with flares and microflares in sheared core fields in active regions, we suspect that the microflaring network core fields are strongly sheared and that their microflares are driven by explosions of the sheared core field as in active regions. Further, as sketched in Figure 7, because the network bipoles are packed among the feet of the coronal funnels, we expect that the network core-field explosions drive heating in the body of the corona in quiet regions and coronal holes in the way that core-field microexplosions drive extended coronal heating in active regions, as sketched in Figure 4. The field configuration of an active network bipole embedded in the foot of a coronal funnel is basically the same as the field configuration for a flaring arch: an active bipole embedded in the end of a larger passive magnetic loop. This suggests that chromospheric spicules, which shoot up from the network magnetic flux concentrations and have the appearance of miniature surges, are the chromospheric component of miniature flaring-arch events driven in the coronal funnels by the exploding core fields embedded in their feet.

Our above inferences (that the magnetic network is peppered with embedded sheared core fields and that, by exploding, these network core fields drive spicules, EUV explosive events, network coronal heating, and extended coronal heating) are predictions to be tested by future high-resolution observations. To this end, we look forward to the Japan/US/UK *Solar-B* space mission scheduled for launch in 2004. *Solar-B*'s 50 cm optical telescope will provide 0.25 arcsec resolution images and spectra of the photosphere and chromosphere, including vector magnetograms with enough sensitivity to the transverse component of the field (~ 100 G) to measure neutral-line magnetic shear in the stronger network bipoles. *Solar-B* will also have EUV and X-ray telescopes that will provide arcsecond resolution of the transition region and corona in coordination with the optical telescope. So we expect *Solar-B* to provide the observations needed to directly test our proposed picture for coronal heating in quiet regions and coronal holes.

In conclusion, the results and considerations of this paper support the view that flares, coronal mass ejections, coronal heating, and spicules are all driven by basically the same thing: exploding sheared core fields. In this picture, confined eruptions and ejective eruptions of sheared core fields occur on all scales ranging from nearly global to subnetwork. Each eruption drives internal heating in the active bipole, and, depending on the configuration of the active bipole and surrounding field, might (1) open the active bipole and eject initially internal field and plasma far out of this bipole, and/or (2) drive heating and surging mass motion in an impacted larger-scale passive magnetic loop or funnel.

This work was funded by the Solar Physics Branch of NASA's Office of Space Science through the Supporting Research and Technology Program and the *SOHO* Guest Investigator Program. S. T. S. is supported by the *Ulysses* and *SOHO* Projects. The picture for coronal mass ejections, flares and coronal heating presented in this paper is compatible with and was partially inspired by an insightful paper by Gold (1964).

APPENDIX A

A MAGNETIC-CONFIGURATION CLASSIFICATION SYSTEM FOR FLARES AND CORONAL MASS EJECTIONS

In this Appendix, we present and discuss in some detail our magnetic-configuration framework for flare and/or coronal mass ejection classification in order to demonstrate its observational basis, the broad range of event types that it covers, and its usefulness for denoting how the pre-event field configuration prevents or allows ejective eruptions and dictates the relation between the coronal mass ejection and the flare heating in ejective events. We want to establish the credence of this framework for sorting out the gross cause-and-effect relations in flares and coronal mass ejections because we take this framework as the starting point for relating nonflare coronal heating to magnetic structure. This framework, together with our quantitative results for coronal heating by magnetic microexplosions in active regions, is the foundation of our view that exploding sheared core fields—in streamer helmets, in active regions, and in the magnetic network—are the drivers of coronal mass ejections, flares, microflares, and the heating of the global corona.

In § 2, we listed six empirical magnetic configurational rules followed by the observed energy release in flare and/or coronal mass ejection events. These rules cover a diversity of event types: single-bipole events and multiple-bipole events, confined events and ejective events. From these rules any flare and/or coronal mass ejection event can be classified in terms of the magnetic bipoles involved and the types and sequence of actions and interactions of these bipoles in the event. The elements of the bipoles and their interactions are indicated schematically in Figure 6. The broadest distinction in this classification is whether the event involves only a single bipole or multiple impacted bipoles. For single-bipole events, there is only one further level of classification: the classification of the energy release as confined or ejective. For multiple-bipole events, there are three subclassifications: first, the classification of each bipole as active or passive; second, the simultaneity or sequence of activation among the bipoles; and third, the classification of each active bipole as confined or ejective.

Because the entire corona is filled with magnetic field, each active bipole, regardless of whether it drives a single-bipole event or a multiple-bipole event, is embedded in surrounding magnetic field. In a multiple-bipole event, some of this adjacent field is in the form of one or more impacted bipoles that partake of the flare heating in the event. In a single-bipole event, all of the field surrounding the active bipole is not only passive (produces no flare heating of its own) but also receives no flare

heating through interfaces with the active bipole. Even so, these unheated adjacent fields should in general have some influence on the active bipole by virtue of being packed against it. In particular, we suppose that the surrounding field together with the internal configuration of the active bipole determines whether the energy release in the active bipole is confined or ejective. The surrounding field will have little influence if it is much weaker than the field in the active bipole. In this case, the energy release will be confined if the sheared core field (the energy source and driver of the release) is strongly enough capped by the envelope of the active bipole; it can be ejective only if the inhibiting envelope field is weak enough relative to the erupting core field. The sketches for the single-bipole events in Figure 6 indicate this difference between confined and ejective events: relative to the sheared core field, the fields enveloping the core are more robust in confined events than in ejective events.

In multiple-bipole events, the energy release in each active bipole is similar to the energy release in single-bipole events in that most of the energy apparently comes from the sheared core field and, partly depending on the surrounding field in which the active bipole is embedded, the release is either confined or ejective. In addition, in multiple-bipole events the energy release in any active bipole is linked to flare heating in one or more other bipoles in contact with that active bipole. Consequently, the overall character of a multiple-bipole event is determined by both the energy releases in the active bipoles and the interactions between the impacted bipoles in the event. In this sense, the elementary building blocks for multiple-bipole events are pairs of interacting impacted bipoles in which at least one bipole is active. The different possibilities for these pairs of interacting bipoles are sketched in the lower part of Figure 6. These sketches depict the general situation in which the two bipoles are of arbitrarily different size, one smaller, one larger. There are then three possible smaller-larger combinations: active-active, passive-active, and active-passive. We will now consider each of these combinations in turn.

In the active-active case, each of the impacted bipoles has a sheared core which supplies most of the energy released in that bipole. The energy release might start spontaneously in one bipole and then trigger the energy release in the other one, or the energy release might begin simultaneously in both, perhaps triggered by onset of reconnection at the interface. In addition, the energy release in either bipole is confined or ejective depending on the circumstances. If both bipoles are embedded deep within the strong closed field of a large active region, then both bipoles will probably have confined releases. If the smaller bipole is part of an active region and the larger bipole is a sheared-core bipole forming the closed helmet under a large streamer, then the energy release in the smaller bipole could produce a confined flare in the active region in close coordination with a coronal mass ejection and long-duration two-ribbon flare produced by the larger bipole. In some instances of this situation, the ejective release in the larger bipole starts first and somewhat later triggers the flare in the active region at one end of the larger bipole. In other instances, the sequence is reversed, the confined flare starting first and triggering the larger bipole to ejectively erupt (an example of such an event, occurring on 1980 July 14, is presented by Machado et al. 1988a).

An ejective release from an active bipole in a multiple-bipole event is basically the same as that in a single-bipole ejective event: the ejective release produces both a coronal mass ejection and a two-ribbon flare in the ejective bipole; the relation between the coronal mass ejection and the flare heating in this bipole is as described in § 2 for long-duration two-ribbon flares. In ejective releases from the sheared-core arcades under large streamers, where the magnetic field is much weaker than in active regions, the flare heating is usually much weaker than in flares in active regions. The flare heating that is produced in one of these large weak-field bipoles in coordination with a streamer-blowout coronal mass ejection can be barely or not at all noticeable in the GOES whole-Sun X-ray flux but still be quite noticeable in coronal X-ray images (e.g., Hiei et al. 1993). If such an ejective release occurs as part of a multiple-bipole event in which a flare is triggered in an active region at one end of the erupting streamer-helmet bipole, then the most noticeable flare heating in the event will be that in the active region. Obviously, the coronal mass ejection has a different relation to the flare heating triggered in the adjacent active-region bipole than to the flare heating in the ejective bipole.

Next there is the passive-active case, the case of a passive bipole impacted against a larger active bipole. Most two-bipole events of this composition are not strikingly different from single-bipole events. The bulk of the flare heating occurs in the active bipole; the passive bipole, being smaller and heated only by leakage from the active bipole, often appears to be a rather insignificant part of the event. When the active bipole is quite large, such as the overall bipole of a large decaying active region, some of the impacted passive bipoles can be comparably large and hence noticeable in coronal images even though the loops that brighten in these passive bipoles remain much dimmer than the flare loops in the active bipole. Examples of such large loops that moderately brighten during the ejective energy release and strong flare brightening in an adjacent larger active bipole can be seen in the *Yohkoh* SXT coronal images of an ejective flare presented by Manoharan et al. (1996) and of another ejective flare presented by Hudson, Acton, & Freeland (1996).

Finally, we come to the active-passive case, the case in which an active bipole is more or less embedded in one polarity of the envelope of a larger passive bipole. An explosive energy release in the active bipole, either confined or ejective, injects energetic particles and heated plasma into a large magnetic arch that is an integral part of the envelope of the passive bipole and that is rooted immediately around the active bipole. The injection is probably accomplished via reconnection between the active bipole and this impacted magnetic arch (Shibata 1996). If the energy release in the active bipole is ejective, then in addition to the injection of particles and heat from the initial interface, some of the erupting core field of the active bipole is ejected up into the leg of the impacted arch. This probably results in more reconnection and more heating of the large arch than when the energy release in the active bipole is confined. For either confined or ejective energy release in the active bipole, the injection of energetic electrons into the large arch during the impulsive phase of the flare in the active bipole immediately produces reverse-slope type III radio bursts and chromospheric and hard X-ray brightening at the far end of the arch (e.g., Tang & Moore 1982; Aschwanden et al. 1992; Hanaoka 1996). When the energy injection is strong enough, a surge can be driven in the large arch: starting during or right after the impulsive electron injection, plasma ranging in temperature from chromospheric to coronal or hotter shoots up along the arch from its driven end; often enough heating occurs that the entire arch becomes illuminated in coronal X-ray images (e.g., Machado et al. 1998b). The events studied and named flaring arches

by Martin & Svestka (1988), Svestka et al. (1989), and Fontenla et al. (1991) are active-passive events of this strong-injection type and in which the active bipole is only four or five times smaller in diameter than the length of the passive arch. If the span of the passive arch is as large or larger than a large active region ($>10^5$ km) and the active bipole is 10 times or more smaller, then the event will probably be identified as a surge in chromospheric/transition-region images and/or as a jet in coronal X-ray images (Tandberg-Hanssen 1977; Shibata et al. 1992).

REFERENCES

Acton, L. W. 1996, in Magnetohydrodynamic Phenomena in the Solar Atmosphere: Prototypes of Stellar Magnetic Activity, ed. Y. Uchida, T. Kosugi, & H. S. Hudson (Dordrecht: Kluwer), 3
Allen, C. W. 1973, Astrophysical Quantities (London: Athlone), 176
Aschwanden, M. J., Bastian, T. S., Benz, A. O., & Brosius, J. W. 1992, ApJ, 391, 380
Cook, J. W., Cheng, C.-C., Jacobs, V. L., & Antiochos, S. K. 1989, ApJ, 338, 1176
Dowdy, J. F., Jr., Rabin, D., & Moore, R. L. 1986, Sol. Phys., 105, 35
Falconer, D. A., Moore, R. L., Porter, J. G., Gary, G. A., & Shimizu, T. 1997, ApJ, 482, 519
Falconer, D. A., Moore, R. L., Porter, J. G., & Hathaway, D. H. 1998, 501, 386
Fontenla, J. M., Svestka, Z., Farnik, F., & Tang, F. Y. 1991, Sol. Phys., 134, 145
Gold, T. 1964, in the Physics of Solar Flares (NASA SP-50), ed. W. N. Ness (Washington, DC: NASA), 389
Gopalswamy, N. 1999, in Proc. Nobeyama Symposium on Solar Physics with Radio Observations (Nobeyama: Nobeyama Radio Obs.), in press
Gosling, J. T. 1993, J. Geophys. Res., 98, 18 937
———. 1995, J. Geophys. Res., 100, 3479
———. 1996, ARA&A, 34, 35
Hanaoka, Y. 1996, Sol. Phys., 173, 319
Harvey, J. W. 1977, in Illustrated Glossary for Solar and Solar-Terrestrial Physics, ed. A. Bruzek & C. J. Durrant (Dordrecht: Reidel), 13
Hiei, E., Hundhausen, A. J., & Sime, D. G. 1993, Geophys. Res. Lett., 20, 2785
Holzer, T. E. 1992, in The Astronomy and Astrophysics Encyclopedia, ed. S. P. Maran (New York: Van Nostrand Reinhold), 336
Hudson, H. S., Acton, L. W., Alexander, D., Freeland, S. L., Lemen, J. R., & Harvey, K. L. 1996, in AIP Conf. Proc. 382, Solar Wind Eight, ed. J. T. Gosling, S. R. Habbal, W. S. Kurth, & M. Neugebauer (New York: AIP), 88
Hudson, H. S., Acton, L. W., & Freeland, S. L. 1996, ApJ, 470, 629
Hudson, H., Haisch, B., & Strong, K. T. 1995, J. Geophys. Res., 100, 3473
Kahler, S. 1987, Rev. Geophys., 25, 663
———. 1992, ARA&A, 30, 113
Kahler, S. W., Moore, R. L., Kane, S. R., & Zirin, H. 1988, ApJ, 328, 824
Karpen, J. T., Antiochos, S. K., & DeVore, C. R. 1996, ApJ, 460, L73
Low, B. C. 1996, Sol. Phys., 167, 217
Machado, M. E., & Moore, R. L. 1986, Adv. Space Res., 6 (6), 217
Machado, M. E., Moore, R. L., Hernandez, A. M., Rovira, M. G., Hagyard, M. J., & Smith, J. B., Jr. 1988a, ApJ, 326, 425
Machado, M. E., Xiao, Y. C., Wu, S. T., Prokakis, Th., & Dialetis, D. 1988b, ApJ, 326, 451
Manoharan, P. K., van Driel-Gesztelyi, L., Pick, M., & Demoulin, P. 1996, ApJ, 468, L73
Martin, S. F., & Svestka, Z. F. 1988, Sol. Phys., 116, 91
Moore, R. L. 1987, Sol. Phys., 113, 121
———. 1988, ApJ, 324, 1132
Moore, R. L., & LaBonte, B. J. 1980, in Solar and Interplanetary Dynamics, ed. M. Dryer & E. Tandberg-Hanssen (Dordrecht: Reidel), 207
Moore, R. L., LaRosa, T. N., & Orwig, L. E. 1995, ApJ, 438, 985
Moore, R. L., Musielak, Z. E., Suess, S. T., & An, C.-H. 1991, ApJ, 378, 347
Moore, R., Porter, J., Roumeliotis, G., Tsuenta, S., Shimizu, T., Sturrock, P. A., & Acton, L. W. 1994, in Proc. Kofu Symposium: A New Look at the Sun, ed. S. Enome & T. Hirayama (Nagano: Nobeyama Radio Obs.), 89
Moore, R., & Rabin, D. 1985, ARA&A, 23, 239
Moore, R. L., & Roumeliotis, G. 1992, in Eruptive Solar Flares, ed. Z. Svestka, B. V. Jackson, & M. E. Machado (Berlin: Springer), 69
Moore, R. L., Schmeider, B., Hathaway, D. H., & Tarbell, T. D. 1997, Sol. Phys. 176, 153
Moore, R., et al. 1980, in Solar Flares, ed. P. A. Sturrock (Boulder: Colorado Associated Univ. Press), 341
Parker, E. N. 1963, Interplanetary Dynamical Processes (New York: Wiley)
Porter, J. G., & Dere, K. P. 1991, ApJ, 370, 775
Porter, J. G., Falconer, D. A., & Moore, R. L. 1998, in Solar Jets and Coronal Plumes, ed. T.-D. Guyene (ESA-SP 421; Noordwijk: ESA), 147
Porter, J. G., & Moore, R. L. 1988, in Solar and Stellar Coronal Structure and Dynamics, ed. R. C. Altrock (Sunspot: National Solar Obs.), 125
Porter, J. G., Moore, R. L., Reichmann, E. J., Engvold, O., & Harvey, K. L. 1987, ApJ, 323, 380
Porter, J., Moore, R., Roumeliotis, G., Shimizu, T., Tsuneta, S., Sturrock, P. A., & Acton, L. W. 1994, in Proc. Kofu Symposium: A New Look at the Sun, ed. S. Enome & T. Hirayama (Nagano: Nobeyama Radio Obs.), 65
Rust, D. M., et al. 1980, in Solar Flares, ed. P. A. Sturrock (Boulder: Colorado Associated Univ. Press), 273
Schrijver, C. J., Title, A. M., van Ballegooijen, A. A., Hagenaar, H. J., & Shine, R. A. 1997, ApJ, 487, 424
Sheeley, N. R., Jr., Howard, R. A., Koomen, M. J., & Michels, D. J. 1983, ApJ, 272, 349
Shibata, K. 1996, in Magnetohydrodynamic Phenomena in the Solar Atmosphere, ed., Y. Uchida, T. Kosugi, & H. S. Hudson (Dordrecht: Kluwer), 13
Shibata, K., et al. 1992, PASJ, 44, L173
Shimizu, T. 1995, PASJ, 47, 251
Spitzer, L. 1962, Physics of Fully Ionized Gases (New York: Wiley)
Sturrock, P. A., ed. 1980, Solar Flares (Boulder: Colorado Associated Univ. Press)
Svestka, Z. 1976, Solar Flares (Dordrecht: Reidel)
Svestka, Z. F., Farnik, F., Fontenla, J. M., & Martin, S. F. 1989, Sol. Phys., 123, 317
Svestka, Z., Jackson, B. V., & Machado, M. E., ed. 1992 (Berlin: Springer)
Tandberg-Hanssen, E. 1977, in Illustrated Glossary for Solar and Solar-Terrestrial Physics, ed. A. Bruzek & C. J. Durrant (Dordrecht: Reidel), 97
Tang, F., & Moore, R. L. 1982, Sol. Phys., 77, 263
Tsuneta, S., et al. 1991, Sol. Phys., 136, 37
Wang, H., Tang, F., Zirin, H., & Wang, J. 1996, Sol. Phys., 165, 223
Withbroe, G. L. 1988, ApJ, 325, 442
Withbroe, G. L. 1992, in The Astronomy and Astrophysics Encyclopedia, ed. S. P. Maran (New York: Van Nostrand), 858
Withbroe, G. L., & Noyes, R. W. 1977, ARA&A, 15, 363
Yoshida, T., & Tsuneta, S. 1996, ApJ, 459, 342